Department of the Navy
Naval Ordnance Test Station
Contract N123(60530)31686A

FREE-SURFACE WATER TUNNEL STUDIES OF A FAMILY OF BASE-VENTILATED HYDROFOILS

J. Brentjes

Hydrodynamics Laboratory
Karman Laboratory of Fluid Mechanics and Jet Propulsion
California Institute of Technology
Pasadena, California

Internal Memorandum E-108.12
Not for General Distribution

Approved by
Taras Kiceniuk

Copy No. 3

June, 1962

TABLE OF CONTENTS

LIST OF FIGURES

LIST OF FIGURES
continued

Purpose of Study

This test program is one of a series designed to investigate the properties of base-ventilated hydrofoils. The purpose of this study was to determine the two-dimensional force and ventilation characteristics of an uncambered hydrofoil which could be truncated by removing four removable trailing edge sections. The program was performed at the request of T. G. Lang of the Naval Ordnance Test Station, Pasadena, who in Reference 1 analyzed the possibilities of reducing the cavity drag of base-ventilated hydrofoils by selecting appropriate section profiles and foil base thicknesses. Using a profile developed in Reference 1, it was intended to study the effects of ventilation air flow rate, angle of attack, and the position of the trailing edge cutoff points, and to compare the experimental values of the drag with those predicted from a linearized flow theory.

Apparatus and Personnel

This program was conducted in the Free-Surface Water Tunnel of the Hydrodynamics Laboratory, California Institute of Technology. The experiment was performed by J. Brentjes who was assisted by L. Whitcanack in obtaining and reducing the data. T. Kiceniuk, who designed the two-dimensional working section, made many valuable suggestions throughout the test program. A close liaison was maintained with T. G. Lang during the test and data analysis to assure that any additions or changes to the original test request were within the scope of the desired results. C. Eastvedt assisted with the photography.

Figure 1 shows the working area of the Free-Surface Water Tunnel with the apparatus and model installed.

Since it was desired to make the study in two-dimensional flow, the two-dimensional insert No. 3 was placed in the tunnel working section. The Laboratory drawing number of these large, plexiglass end-plates is N-3296 YY. The plates are mounted to a rigid, stainless steel structure which can be bolted to the bottom of the working

section. Prior to undertaking this hydrofoil test program, it was decided to make a survey of the flow characteristics between these endplates. A detailed description and analysis of the water surface contour, upflow, and boundary layer thickness are presented in Appendix C.

The Task MK II strain-gage balance was used to measure the model forces. This balance was supported by the elevating mechanism on the top of the tunnel working section. This hand operated elevating mechanism allows a model to be raised or lowered from the water surface with a repeatability of .001 feet.

The force readout system used with the Task MK II balance was designed by Shapiro and Edwards, South Pasadena. It is only a temporary system which will be modified and expanded in the near future. Figure 2 shows the schematic diagram of the components. The voltage source for each force cell is a set of three Mallory mercury batteries with a total voltage output of four volts. The sensitivity adjustment at the bridge output was used for calibration purposes. With the selector switch, each force component could be read in turn. Because the digital voltmeter was not capable of tracking the force fluctuations picked up by the balance, a filter-amplifier system was designed which would filter out these high frequency fluctuations. This filtered signal was then fed to the Kintel pre-amplifier and digital voltmeter, and finally registered by the digital readout.

The ventilation of the foil base was attained by bleeding pressurized air through a strut-mounted probe located aft of the model. This thick strut was positioned downstream of the two-dimensional endplates in order to eliminate the blockage effects which would have occurred if it had been placed in the narrow channel. The probe tip was flattened somewhat to avoid interference in the flow leaving the trailing edges of the foil. This same arrangement also incorporated a thin tube for measuring the cavity pressures. Figure 3 is a drawing of the probe. Figure 4 shows the flow diagram of the bleed air

and cavity pressure tap. A detailed description of the method used to measure static pressures in water where complete or incomplete ventilation occurs is presented as a separate topic in Appendix A.

The air flow rate into the foil base cavity was measured with the Fisher and Porter Flowrator (Serial No. J1-2154). The aluminum float for this Flowrator was used only for the configuration called number one cutoff, (see Table I, Page 31 and Figure 5) which has the thinnest trailing edge section. The stainless steel float was used for the blunter truncated sections which required larger amounts of bleed air for full ventilation. Calibration curves for both floats are presented in Figures 6 and 7. The air supply pressure was measured with a Heise pressure gage (Serial No. H1667) which has a range of 0 to 30 psig.

Photographs were taken with a Kodak 4 x 5 Master View Camera using an exposure time of 1/5 second and f: 16. The film was Royal Pan. Four DXR flood lamps were used for back lighting and two 750 watt spot lights were used for front lighting. During the preliminary runs a few electronic flash photographs were taken of the number four cutoff model. Two FT-125 flash lamps with a flash duration of 3 to 4 microseconds were used for back lighting.

Description of Model

The model used in this experiment is one of a series of base-ventilated hydrofoils proposed by T. G. Lang (Reference 1). Using the linearized expression for cavity drag as derived by M. P. Tulin (Reference 2) a profile was proposed by T. G. Lang which would have zero cavity drag when the ventilation number , K, is equal to zero. The contour is given in Reference 1 by the general equation:

$$y = .525\, t_o \left[1.70 \sqrt{\frac{x}{c'}} - \left(\frac{x}{c'} \right)^2 \right] \qquad (1)$$

where:

y = abscissa from chord line to upper and lower surface

x = distance along chord from leading edge

t_o = maximum foil thickness

c' = chord of foil cutoff at point for zero cavity drag.

The profile given by the above equation can be extended to form a streamlined foil so that $y = 0$ at the trailing edge. Hence, for $x = c$ (the chord of the streamlined foil):

$$1.70\sqrt{\frac{c}{c'}} - \left(\frac{c}{c'}\right)^2 = 0$$

$$\text{or} \quad c = c' \, (1.70)^{2/3}$$

The foil used in this program has a 15% thickness-chord ratio; the chord being the distance from the leading edge to the trailing edge where $y = 0$. This chord was chosen to be four inches, so that $c' = 2.83$ inches and $t_o = .60$ inches, and the particular profile is given by

$$y = .315\left[1.70\sqrt{\frac{x'}{2.83}} - \left(\frac{x}{2.83}\right)^2\right]$$

The coordinates and sketch of this profile are shown in Table I on Page 31 . Both the chord and span are four inches.

In order to determine the effect of ventilation on the drag when the foil has its trailing edge at $x = c' = 2.83$ inches, as well as other distances x, the model was designed so that sections could be removed progressively from the back. These sections were located and held in place by two dowel pins and two screws (see Figure 5.)

The cutoffs were taken at values of $\frac{x}{c}$ = 60%, 70%, 80%, and 87.5%.

It was originally considered important to shield the strut from the large tare forces by surrounding the strut and air and pressure tubes by an aluminum extruded fairing. However, it was found in Reference 4 that the bulky shield created a pressure field which could radically alter the force characteristics of the foil. For this reason, the foil was modified so it could be mounted to a ten inch long strut with a chord of 2.25 inches and the thin NACA 16-006 section profile. The top of this strut fits into the angle adjustment yoke of the Task strain-gage balance. No fillets were used at the foil-strut intersection, and the foil tips were not faired. The material used for the foil was leaded brass.

Experimental Procedure

With the model and angle of adjustment yoke mounted to the strain-gage balance, a calibration of the readout system was made. To calibrate the drag a strong string was tied around the leading edge of the strut and guided over a pulley which was clamped parallel to the tunnel walls. With the string parallel to the balance centerline, weights were hung on its end for calibration. By adjusting the sensitivity potentiometer, the voltage reading of the digital voltmeter could be made to read 1.000 millivolt = 1.000 pound.

To calibrate the normal force cell N_1, weights were hung by means of a string directly over the cylindrical sleeve. In order to put the weights directly over the electrical centerline of the force cell N_1, the string was positioned such that the output of N_2 would remain constant with large changes in the applied load at N_1. Then the d. v. m. readings were again made to correspond to 1.000 millivolt = 1.000 pound. During the preliminary trial runs it was found that over long periods of time these values would vary as much as 2% due to drift in the battery voltage and potentiometer settings. For this reason,

calibration checks were made regularly during the course of the experiment.

Adjusting the foil and end-plates to minimize the clearance between the foil tips and windows was a very long and tedious procedure. With the model support, balance and elevating mechanism clamped down rigidly, each of the large end-plates was positioned so that the foil, when changing the angle of attack and depth of submergence, would not touch the walls. Since a change in angle of attack results in rotation of the foil about the transverse horizontal centerline of the balance, it is important to have the foil tips accurately perpendicular to this balance centerline. The final clearance between each foil tip and wall was held at . 009 inches when the water was at rest in the tunnel. Since this narrow gap was very much smaller than the boundary layer thickness along the wall (see Appendix C), it was believed that the tip effects would thus be essentially eliminated. However in later studies with the two-dimensional test section, it was found that because of pressure differences between the two sides of the two-dimensional working section windows, the windows bowed and created a greater gap when the tunnel was operating than when the water was stationary. This increase in gap clearance was not accounted for in this program. A later study by E. R. Bate, Jr. (Reference 9) with the same foil and test section showed that the foil data was significantly altered. Particularly, the lift was effected by the increased gap clearance.

First the streamlined foil with no cutoff was tested. After obtaining the zero readings of the forces at all the angles of attack (-6° to $+6^{\circ}$ in 2° increments), the foil was run at three velocities (10, 15 and 20 fps) and a depth of approximately eight inches. The ventilation probe was not installed for these runs.

Then the foil with the number two cutoff was tested. For this, the ventilation probe was mounted behind the foil such that the air exhausted about 1/4 inch from the foil base. The pressure tap was

therefore approximately 3/8 inch behind the base. This adjustment of probe position had to be made for every change in angle of attack. With the required angle of attack set and with the probe positioned, the zero readings were taken. Then the tunnel was brought up to speed (20 fps) and the forces and base pressure were recorded at the zero air flow rate. Subsequently, the bleed air valve was opened to obtain various values of cavity lengths and again the forces, base pressure, bleed air pressure, and air flow rate readings were taken. Finally when several values of air flow rate readings were recorded, the tunnel was stopped and the zero readings were noted again. This procedure was repeated for all angles of attack and the other cutoff trailing edge sections.

Since the air flow rates for the number one cutoff were relatively small, the aluminum float was used in the Flowrator. This made it possible to obtain larger and more accurate readings from this instrument.

At the high angles of attack, and particularly for the large cutoff sections, it was not possible to obtain many values of air flow rate. Under those conditions the cavity became very unstable and would jump forward on the upper surface of the foil along the strut-foil intersection. The probe itself would then begin to vibrate violently, so that the air flow rate had to be reduced to prevent possible damage to the probe. Even for the small cutoffs and low angles of attack the tip of the probe would sometimes interfere with the shape of the air cavity. For cavity lengths greater than about 2 1/2 inches the air would completely surround the thick part of the probe (see Figure 11).

It was suggested by T. G. Lang that the jet of air issuing from the probe and impinging on the foil base could effect the drag. For this reason, a brief test was made in air with the largest cutoff model. To simulate the cavity shape, thin paper was extended from the upper and lower surface trailing edges and the probe mounted between this. In this way the "jet effect" was found to be very small, for, even at a

flow rate coefficient of .06, the thrust was only .007 pounds, which is about 1 1/2% of the minimum foil drag.

Because the probe could not be mounted extremely close to the model base, the pressure tap was not always directly inside the cavity, thus possibly causing somewhat erroneous cavity pressure reading. This, however, occurred only for the number one cutoff and smaller air flow rates. When the foil was in the fully wetted condition the pressure behind the foil base was so low that the manometer went off scale, indicating that the pressure head was more than 1.6 feet of water below atmospheric.

Photographs were taken for the four cutoffs at various angles of attack and air flow rates. Pages 39, 40 and 41 present some of these photographs for typical data runs. Prints of the other photographs listed on pages 12 and 13 are on file in the Laboratory.

Finally, the strut was tested by itself to determine its drag and the influence of any blockage effect due to the parallel end-plates. The drag data was taken at various strut rake angles, depths of submergence and a velocity of 20 fps. The results of this measurement, performed in both the two-dimensional test section and in the open channel are presented in Figure 12.

Analysis of Data

In order to assure that the data was consistent and did not exhibit any unexpected trends, all of the data was partly reduced and plotted during the runs. The strut tare drag was plotted in Figure 12 which also shows the effect of blockage. The foil drag and lift forces were calculated and plotted for each cutoff section. Figures 13 through 17 present L' and D' as functions of indicated angle of attack and for various conditions of cavity length. It was found in the preliminary investigations of the flow between the two-dimensional end-plates that because of boundary layer growth along the walls a certain amount of rise in the water surface was created. This resulted in a change of

direction of the water velocity. At a velocity of 20 fps and a depth of about eight inches the angle of upflow, α_o, was approximately 3.0° (Appendix C). The graphs of L' versus indicated angle of attack show that the angle of zero L' is approximately minus 3°. Since this is an uncambered section, this suggests that a correction be made for the angle of attack. The true drag and lift are related to α_o as shown below:

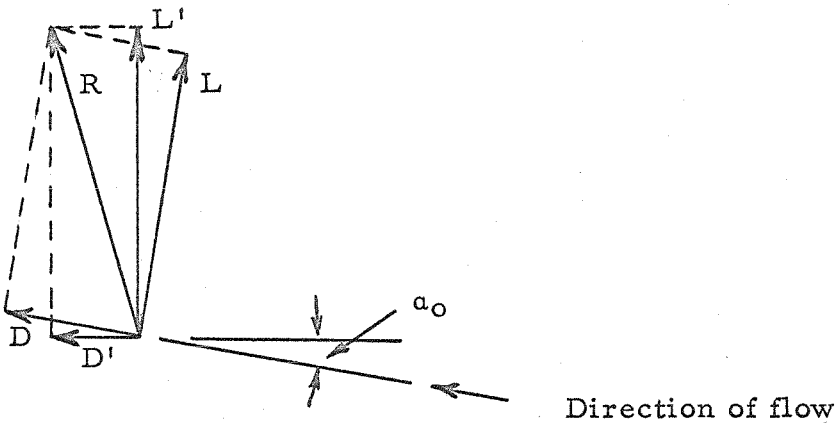

The formulas for L and D are:

$$L = L' \cos \alpha_o - D' \sin \alpha_o$$

and

$$D = L' \sin \alpha_o + D' \cos \alpha_o$$

In addition, it is suggested that in this force data analysis the effects of blockage, boundary layer thickness and strut interference be considered also. As was noted before, the gap clearance under operating conditions was increased by a significant amount. Later studies with this foil have shown that the lift curve slope is about 2π when this gap is made very small(Reference 9).

The cavity lengths, as indicated on the lift and drag curves, were only estimated and noted in order to obtain approximately the same cavity size at each angle of attack. The effect of ventilating the foil base on drag is very distinct. Even for the large cutoff sections, where abrupt ventilation along the foil-strut intersection would occur, the drag data was reasonable consistent. Because of the upper surface ventilation, the lift shows some dropoffs for the longer cavities.

The air flow rates were reduced to coefficient form using the

method described in Appendix B. Figure 18 shows the drag of each cutoff section as a function of air flow rate coefficient. This graph is for $\alpha_{ind} = 0^{o}$. The data appears to be quite consistent and shows that the minimum drag does not occur with the number three cutoff (as predicted in Reference 2) but with the number one cutoff. However, the latter was not at K = 0. Consider the plot of ventilation number versus air flow rate coefficient (Figure 19). For the numbers one and two cutoffs the ventilation number was negative, so that the higher cavity pressure for these two cutoffs cause a forward thrust component. When the drag is increased by $A_b (P_c - P_o)$, the values correspond very closely to those for the model with no cutoff sections.

Actually, the method used to ventilate the base and measure the base pressures was very unsatisfactory. The interference of the probe and the position of the pressure tap undoubtedly created erratic cavity shapes and pressure readings. Small variations in the bleed air pressure through the cavity pressure line (as discussed in Appendix A) were likely to occur also. Figure 20 shows the ventilation number versus air flow rate for all the angles of attack. The data points show considerable scatter, and there seems to be no particular variation with angle of attack. If, in the future, a more detailed study of the ventilation characteristics is to be made, it is suggested that the model be mounted rigidly between the walls - without the strut - and that the bleed air and pressure tap be brought through the sides directly to the foil base. In this way, the interference will be eliminated.

REFERENCES

1. Lang, T. G., "Base-Ventilated Hydrofoils, "NaVord Re port 6606, NOTS TP 2346, Oct. 19, 1959.

2. Tulin, M. P., "Steady Two-Dimensional Cavity Flows About Slender Bodies," Carderock, Md., DTMB Rep. 834, May, 1953.

3. Lang, T. G., and Daybell, D. A., "Free-Surface Water Tunnel Tests of an Uncambered Base-Vented Parabolic Hydrofoil of Aspect Ratio One," NOTS TN P5015-22, March, 1962.

4. Brentjes, J., "The Interference Effects of the Alcoa Section Shield on the NOTS Parabolic Hydrofoil Drag," Exp. Memo. E-118.2M, Hydrodynamics Laboratory, California Institute of Technology, March, 1962.

5. Pankhurst, R. C., and Holder, D. W., "Wind Tunnel Technique," Pitman and Sus, London, 1952, p. 325-396.

6. Mendelsohn, R. A., and Polhamus, J. F., "Effect of the Tunnel-Wall Boundary Layer on Test Results of a Wing Protruding from a Tunnel Wall." NACA TN 1244, April, 1947.

7. Ripken, J. F., "Interference Effects of a Strut on the Lift and Drag of a Hydrofoil, "St. Anthony Falls Hydraulic Laboratory, P. R. 65, August, 1961.

8. Schlichting, H., "Boundary Layer Theory." Pergamon Press, New York, 1955.

9. Bate, E. R. Jr., "The Effect of Gap Clearance and Support Strut Interference on the Lift Curve Slope of a Hydrofoil." Hydrodynamics Laboratory, California Institute of Technology, Pasadena, California, Internal Memorandum E-118.14M, November, 1962.

10. Gadd, G. E., "An Air-Blowing Technique for Measuring Pressures in Water." National Physical Laboratory, Ship Division, October 18, 1961.

LIST OF PHOTOGRAPHS

Report Fig. No.	Pict. No.	Run No.	Neg. No.	Cutoff No.	α	Q'	Remarks
	1	16	10865	4	+2°		Data not presented nor analyzed. V = 15fps (flash photographs.)
	2	13	10866	4	+2°		
	3	14	10867	4	+2°		
11b	4	18	10868	4	+2°		
10a	5	29	10870	2	-6	.00645	
	6	24	10871	2	-4	.00842	
	7	20	10872	2	-2	.0077	
	8	2	10873	2	0	.00754	
	9	7	10874	2	+2	.0098	
	10	12	10875	2	+4	.00768	
	11	17	10876	2	+6	.00645	No good.
	12	17	10877	2	+6	.00645	
	13	34	10878	3	+6	.0047	
9a	14	37	10879	3	+4	.00562	
	15	42	10880	3	+2	.0047	
	16	48	10881	3	0	.00852	
	17	50	10882	3	0	.0346	Some tip effects.
	18	52	10883	3	-2		
	19	57	10884	3	-4	.00471	
	20	62	10885	3	-6	.00824	
9b	21	65	10886	3	-6	.0417	Upper surface ventilation
	22		10887	3			Static Water
	23	68	10888	4	0	.00398	
	24	73	10889	4	+2	.00395	
	25	75	10890	4	+2	.0270	

LIST OF PHOTOGRAPHS
continued

Report Fig. No.	Pict. No.	Run No.	Neg. No.	Cutoff No.	α	Q'	Remarks
	26	78	10891	4	+4	.00473	
	27	78	10892	4	+4	.00473	
10b	28	83	10893	4	+6	.0069	
	29	86	10894	4	-2	.0104	
	30	88	10895	4	-2	.0391	Long cavity
	31	91	10896	4	-4	.01118	
	32	94	10897	4	-4	.0410	
	33	97	10898	4	-6	.00697	
	34						No record
	35	99	10899	4	-6	.0256	
	36	111	10900	1	+2		Erroneous with steel float
	37	115	10901	1	+2	.0336	
	38	120	10902	1	+4	.01279	
11a	39	121	10903	1	+4	.1183	Ventilation near strut
8a	40	126	10904	1	0	.01116	
	41	137	10905	1	-2	.0287	
	42	144	10906	1	-4	.0258	
8b	43	149	10907	1	-6	.0296	
	44	151	10908	1	-6	.0826	
	45		10917				Picture of model

DATA SUMMARY SHEET

Run No.	Experiment	Angle of Attack	Velocity fps	Cavity Length
1^A - 21^A	zero cutoff	-6° to $+6^\circ$	10, 15, 20	zero
1 - 32	#2 cutoff	-6° to $+6^\circ$	20	0", 1/2", 3/4", 1", 1-1/2"
33 - 66	#3 cutoff	-6° to $+6^\circ$	20	0", 3/4", 1", 1-1/2", 2", 3"
67 - 100	#4 cutoff	-6° to $+6^\circ$	20	0", 1", 1-1/2", 1-3/4", 2", 2-1/2", 3", 7
101 - 109	#4 cutoff re-runs	0°, 2°	20	0", 1", 1-1/2", 7
110 - 152	#1 cutoff	-6° to $+6^\circ$	20	0", 1/4", 1/2", 3/4", 1"
8^B - 21^B	#4 cutoff add. data	-6° to $+6^\circ$ 0	20	zero 3/4", 1", 1-1/2", 6", 8"
153 - 208	strut drag	-6° to $+6^\circ$	20	zero
209 - 212	airjet thrust	0	zero	zero

Parabola Circular Arc Hydrofoil F.S.W.T. JAN. 24, 1962
0% cut off (NON vented) J.B & E.W

RUN NO	α	hIND	DIND	N_1 IND	N_2 IND	Remark
	$+6^\circ$	.330	-.241	-.26	+2.07	water level 1.65
	$+4^\circ$	"	-.235	-.03	+1.84	Zero
	$+2^\circ$	"	-.227	+.20	+1.63	
	0	"	-.229	+.42	+1.40	
	-2°	"	-.229	+.64	+1.16	
	-4°	"	-.229	+.87	+.95	
	-6°	"	-.228	+1.08	+.71	
1^A	-6°	"	+.052	-.07	+.40	V=10FPS hREF=8.8inch
2^A	-4°	"	-.003	+.30	+1.26	
3^A	-2°	"	-.012	+.77	+1.95	
4^A	0	"	-.039	+1.57	+2.63	
5^A	$+2^\circ$	"	-.038	+2.69	+3.23	
6^A	$+4^\circ$	"	-.010	+4.11	+3.64	
7^A	$+6^\circ$	"	+.040	+5.52	+3.72	
8^A	$+6^\circ$	"	+.464	+12.00	+5.93	V=15FPS hREF 8.31inch
9^A	$+4^\circ$	"	+.328	+8.18	+5.61	
10^A	$+2^\circ$	"	+.237	+4.94	+4.95	
11^A	0°	"	+.204	+2.31	+3.86	
12^A	-2°	"	+.210	+.49	+2.60	
13^A	-4°	"	+.281	-.83	+1.30	
14^A	-6°	"	+.405	-1.96	-.65	
15^A	-6°	"	+.856	-4.32	-2.00	V=20FPS hREF=8.0"
16^A	-4°	"	+.650	-2.16	+1.45	
17^A	-2°	"	+.547	+.27	+3.56	
18^A	0°	"	+.532	+3.86	+5.85	
19^A	$+2^\circ$	"	+.633	+8.17	+7.44	
20^A	$+4^\circ$	"	+.809	+13.56	+8.35	
21^A	$+6^\circ$	"	+1.134	+19.90	+8.72	
	$+6^\circ$	"	-.222	-.27	+2.09	Zero
	$+4^\circ$	"	-.220	-.03	+1.88	to be used in
	$+2^\circ$	"	-.218	+.19	+1.65	analysis of V=20 fps
	0	"	-.218	+.41	+1.41	
	-2°	"	-.220	+.64	+1.17	
	-4°	"	-.222	+.86	+.96	
	-6°	"	-.218	+1.08	+.73	

Parabola Circular Arc Hydrofoil

#2 cut-off

2-8-62

J.B. & F.W.

U = 20 FPS

Run No	α	D, Ind	N_1, Ind	N_2, Ind	P_b PSIG	P_c Ft H_2O	Q, Ind	l_c IN	Picture No	Remark
		4.004	3.900	3.900						Battery
	0°	-.388	+11.25	+1.83	20.4	.605	—	—		W.L. 609 Zero
1	0°	+.836	+13.05	+8.24	20.4	-.56	0	0		hrer-846
2	0°	+.432	+13.97	+7.10	18.6	+.690	1.5	.50	8	
3	0°	+.374	+13.93	+6.83	18.7	+.81	9.5	.75		
4	0°	+.342	+13.93	+6.67	18.3	.90	19.0	1.00		
5	0°	+.275	+14.03	+6.46	17.7	.98	41.0	1.50		
Zero	0°	-.386	+11.23	+1.84	20.8	—	—	—		
Zero	+2°	-.400	+11.02	+2.06	21	.605	—	—		
6	+2°	+.712	+17.49	+9.53	20.9	-.06	0	0		
7	+2°	+.393	+18.39	+8.83	18.6	.65	2.5	.50	9	
8	+2°	+.344	+18.49	+8.69	18.6	.74	8.0	.75		
9	+2°	+.235	+18.58	+8.28	18.3	.930	11.5	1.00		
10	+2°	+.180	+18.66	+8.09	17.9	1.010	30.0	1.50		
Zero	+2°	-.410	+11.02 +11.01	2.06	21	.605				
Zero	+4°	-.419	+10.78	+2.28	21	.605	—	—		
11	+4°	.761	+22.76	+10.24	20.9	-.20	0	0		D= .746-.763
12	+4°	.450	+23.42	+9.44	18.5	.67	1.5	.50	10	D= .448-.457
13	+4°	-.393	+23.53	+9.28	18.8	.77	7.0	.75		D= .390-.397
14	+4°	.408	+23.59	+9.27	19.2	.86	10.0	1.00		D= .379-.413
15	+4°	.787	+22.78	+10.92			—	—		
				Q>10, unstable ventilation near strut						
		4.20	10.78							
Zero	+4°	-.422	+10.79	+2.29	21	.605	—	—		

Parabola Circular Arc Hydrofoil.
#2 cut-off

2-8-62 J.B. & F.W.

V = 20 ft/s

Run No.	α	Dind.	N ind	M ind	P_t Pitot	P_c Hub	Quad	ℓ_c in		Remarks
zero	+6°	-.425	+10.57	+2.49	20.7	—	—	—		
16	+6°	+.849	+28.42	+9.96	20.9	+.24	0	0		D .842-.85
17	+6°	+.572	+27.92	9.06	18.7	.70	1.0	.50	11212	.569-.58
18	+6°	+.874	28.46	10.04	20.9	+.24	0	0		.865-.88
Zero	+6°	-.425	+10.55	+2.49	20.7	—	—	—		
			Q > 1.0 large ventilation near strut							
Zero	-2°	-.420	+11.41	+1.62	20.7	—	—	—		
19	-2°	+.836	+9.72	+5.80	20.8	+.23	0	0		D 829-83
20	-2°	.452	+10.59	+4.72	18.4	+.75	1.5	.50	7	452-47
21	-2°	.417	+10.73	+4.58	18.6	.78	8.0	.75		.404-.43
22	-2°	.405	+10.63	+4.45	19.0	.81	20.0	1.00		.402-41
22A	-2°	.869	+9.64	+5.81	20.8	.23	0	0		
Zero	-2°	-.418	+11.40	1.63	20.7	—	—	—		
Zero	-4°	-.419	+11.62	+1.40	20.7	—	—	—		
23	-4°	1.000	+7.25	+3.20	21	-.10	0	0		D .997-1.0
24	-4°	.623	+8.21	+2.24	18.8	.73	2.0	.50	6	—
25	-4°	.607	+8.27	+2.20	18.5	.76	7.5	.75		—
26	-4°	.561	+8.46	+2.17	18.0	.80	25.5	1.00		555-60
27	-4°	1.033	+7.19	3.22	21	-.10	0	0		—
Zero	-4°	-.413	+11.61	1.41	20.7	—	—	—		
Zero	-6°	-.417	+11.85	+1.18	20.7	-.605	—	—		
28	-6°	+1.361	+4.97	-.95	21.1	-.036	0	0		—
29	-6°	+.976	+5.91	-1.43	18.8	+.63	1.0	.50	5	D 962-97
30	-6°	+.895	+6.08	-1.62	18.4	+.76	5.0	.75		891-917
31	-6°	+1.920	+6.13	-1.83	19.5	.80	10.0	1.00		886-92
32	-6°	+1.405	+4.97	-1.38	21.1	-.140	0	0		—
Zero	-6°	-.412	+11.85	+1.18	20.7	.605	—	—		

Parabola Circular Arc HydroFoil
#3 Cut OFF

2-9-62
J.B. + L.W. 18

V = 20 FPS

RUN NO	α	D IND	N_1 IND	N_2 IND	P_b PSIG	P_c FT H_2O	Q_{IND}	l_c IN	Picture NO	Remark
Zero	+6°	-.475	+10.49	+2.53	23.3	.595	—	—		W.L. 163
33	+6°	+1.236	+9.96	+25.06	23.3	-.95	0	0	1	
34	+6°	+.720	+8.61	+25.39	18.6	.125	1.0	.75	13	D .675-.741
35	+6°	+1.264	+10.17	+25.12	23.3	-.95	0	0		1.244-1.280
Zero	+6°	-.475	+10.49	2.55	23.3	.595	—	—		
Zero	+4°	-.477	+10.73	+2.33	22.8	.595	—	—		
36	+4°	+1.162	+10.35	+19.80	23.0	<-1.0 OFF SCALE	0	0		D 1.160-1.180
37	+4°	+.562	+21.29	+8.91	18.5	+.24	1.5	1.0	14	
38	+4	+.386	+21.62	+8.44	18.5	.48	13.5	1.5		
39	+4°	+.304	+21.70	+8.10	18.7	.63	19.0	2.0		
40	+4°	+1.166	+10.33	+19.83	22.9	<-1.0 OFF SCALE	0	0		D 1.155-1.185
Zero	+4°	-.476	+10.71	+2.39	23.5	.595	—	—		
Zero	+2°	-.480	+10.92	+2.09	23.1	.600	—	—		W.L. 164
41	+2°	+1.045	+15.52	+9.70	22.0	-.93	0	0		
42	+2°	+.501	+16.76	+8.43	18.7	+.10	1.0	1.0	15	D .495-.520
44	+2°	+.400	+17.11	+8.13	18.5	.34	12.0	1.5		D .395-.410
45	+2°	+.292	+17.35	+7.81	18.3	.53	20.0	2.0		—
46	+2°	+1.080	+15.55	+9.84	22.0	-.93	0	0		
Zero	+2°	-.486	10.89	+2.13	23.1	.600	—	—		
Zero	0°	-.511?	+11.14	+2.02	23.1	.590	—	—		
47	0°	+1.052	+11.72	+8.46	20.7	-.62	0	0		
48	0°	+.541	+13.08	+7.24	18.8	+.15	4.5	1.0	16	
49	0°	+.342	+13.39	+6.69	19.9	+.45	21.5	1.5		
50	0°	+.293	+13.59	+6.28	18.9	+.58	26.5	2.0	17	.184-.228
51	0°	1.105	+11.74	+8.64	22.	-.60	0	0		1.105-1.125
Zero	0°	-.482	11.08	2.01	23.1	.590	—	—		

Pict. 17 shows some tip effects

Parabola Circular Arc Hydrofoil
#3 Cut-OFF

2-7-68
S.B & D.W 19

U = 20 FPS

Run No	α	D_{lwd}	N_{1-lwd}	N_{2-lwd}	P_b PSIG	P_c Ft H_2O	Q_{lwd}	l_c IN	Pictures	Remarks
Zero	-2°	-.486	+11.26	+1.74	22.1	.590	—	—		
52	-2°	+1.160	+8.67	+6.54	22.8	-.63	0	0		
53	-2°	+1.603	+9.82	+5.20	18.5	+.21	7.5	1.0	18	D 590-621
54	-2°	.512	+10.07	4.85	18.5	.38	16.5	1.5		640-52
55	-2°	1.163	+8.62	+6.55	22.8	-.63	0	0		
		Q > 17.5, large tip effects								
Zero	-2°	-.468	+11.29	1.77	22.1	.590	—	—		
Zero	-4°	-.480	+11.50	+1.56	22.6	.590	—	—		
56	-4°	1.364	+6.13	+4.18	22.5	-.69	0	0		hyst = 8.7
57	-4°	+.927	+7.25	+3.16	18.5	+.08	1.0	.75	19	
58	-4°	+.813	+7.50	+2.83	18.2	+.20	8.0	1.0		
59	-4°	+.657	+7.86	+2.54	18.1	.38	15.5	1.5		
60	-4°	1.411	6.10	4.26	23.6	-.70	0	0		
		Q > 15.5 tip effects & supercavitation, unstable N_1 and N_2								
Zero	-4°	-.455	11.51	1.57	22.6	.590	—	—		
Zero	-6°	-.467	+11.64	+1.35	23.5	.605	—	—		
61	-6°	+1.772	+4.07	+1.21	22.3	OFF scale	0	0		D 1.757-178
62	-6°	+1.132	+5.37	-.33	19.0	-.05	3.5	.75	20	D 1.129-1.14
63	-6°	+1.055	+5.66	-.64	18.8	.22	10.0	1.00		.859-85
64	-6°	+.850	+6.09	-1.24	18.7	.50	13.5	2.00		
65	-6°	+.826	+6.26	-1.43	18.1	.60	32.5	3.00	21 →	cone supercavitation
66	-6°	1.813	3.82	-1.33	23.0	OFF scale	0	0		D 757-89
Zero	-6°	-467	+11.72	+1.36	23.5	.605	—	—		
	U = 0	Showing Pressure Tap & Blocked in							22	

Parabola Circular Arc Hydrofoil
#4 Cut-OFF

2-12-62
J.B. + L.W.[20]

U = 20 FPS

Run No.	α	D_{ind}	$N_{1\,ind}$	$N_{2\,ind}$	P_b psig	P_c ft H_2O	Q_{ind}	l_c in	Picture No	Remark
Battery voltage		3.959	3.807	3.679						
Zero	0°	-.502	+11.70	+2.46	22.8	.605	—	—		
67	0°	+1.747	+10.27	+10.30	22.5	OFF-scale	0	0		
68	0°	+1.012	+12.14	+8.40	18.6	-.43	1.0	1.0	23	D .900-1.0
69	0°	+.870	+12.37	+8.13	18.4	-.235	7.0	1.5		
70	0°	+.585	+13.04	+7.57	18.9	+.078	24.0	2.5		D .581-.601
71	0°	1.753	10.20	+10.37	22.3	OFF-Scale	0	0		
Zero		-.508	+11.68	+2.47	23.9	.605	—	—		
Zero	+2°	-.508	+11.51	+2.64	23.4	.605	—	—		
72	+2°	+1.746	+13.67	+11.41	22.8	OFF scale	0	0		D 1741-176
73	+2°	+1.012	+15.30	+9.45	18.9	-.45	1.0	1.0	24	
74	+2°	+.713	+16.13	+8.75	18.5	-.12	10.0	1.5		D .707-.72
75	+2°	+.551	+16.05	+7.93	18.9	+.13	24.0	2.5	25	D 1752-178
76	+2°	1.782	+13.62	+11.44	22.8	OFF-scale	0	0		
Zero	+2°	-.507	+11.50	+2.64	23.4	.605	—	—		
Zero	+4°	-.507	+11.32	+2.84	23.4	.605	—	—		
77	+4°	+1.640	+18.32	+11.31	22.9	OFF scale	0	0		D 1617-1.66
78	+4°	+1.840	+19.99	+9.31	19.0	-.28	1.5	1.0	26&27	
79	+4°	+.756	+20.14	+9.01	18.5	-.14	5.0	1.5		D .756-.766
80	+4°	+.653	+18.30	8.08	18.2	+.07	26.0	2.5		D .649-.658
81	+4°	+1.643	+18.31	+11.30	22.9	OFF scale	0	0		D 1.644-1.66
Zero	+4°	-.497	+11.32	+2.83	23.4	.605	—	—		
Battery voltage		3.959	3.815	3.673						

Parabola Circular Arc Hydrofoil
#4 Cut-off

2-13-62
J.B. & L.W.

U = 20 FPS

Run No.	∠	D_{wd}	W_1 wd	W_2 wd	P_b psig	$R_{E_{H_2O}}$	Q_{wd}	l_c in	Picture No.	Remarks
Battery Volt.		3.949	3.642	3.690						
Zero	+6°	-.526	+10.74	+3.08	22.1	.605	—	—		W.L.=1.6
82	+6°	+1.692	+22.17	+11.26	22.2	off-scale	0	0		
83	+6°	1.079	+22.70	+9.35	19.1	-.25	4.0	1.0	28	
84	+6°	1.712	22.22	11.18	22.2	off-scale	0	0		
		Q > 4.0	large ventilation, wear strut							
Zero	+6°	-.512	+10.74	+3.11	22.2	.605	—	—		
Zero	-2°	-.528	+11.45	+2.36	22.5	.605	—	—		
85	-2°	+1.640	+7.60	+8.51	21.7	off-scale	0	0		D 1.635-1.6
86	-2°	+.995	+9.06	+6.90	19.4	-.39	7.0	1.0	29	
87	-2°	+.711	+9.73	+6.11	18.8	-.04	25.5	1.5		D .284-.33
88	-2°	+.307	+10.30	+4.98	18.2	+.150	37.5	7.0	30	W .900-10.2
89	-2°	1.702	+7.46	+8.54	21.7	off-scale	0	0		
Zero	-2°	-.510	+11.46	+2.39	22.5	.605	—	—		
Zero	-4°	-.509	+11.73	+2.24	21.3	.61	—	—		W.L.=1.6
90	-4°	+1.915	+5.24	+6.57	21.5	off-scale	0	0		
91	-4°	+1.201	+6.75	+4.61	18.8	-.44	8.0	1.0	31	
92	-4°	+1.025	+7.15	+4.11	18.3	-.22	20.5	1.5		D .999-1.03
93	-4°	+.910	+7.45	+3.85	18.1	-.05	27.5	1.75		
94	-4°	+.675	+7.07	+1.65	18.3	+.38	40.0	7.0	32	
95	-4°	1.966	+5.07	+6.69	21.5	off-scale	0	0		
Zero	-4°	-.512	+11.73	+2.25	21.3	.61	—	—		
Zero	-6°	-.520	+11.91	+2.09	21.3	.61	—	—		
96	-6°	+2.301	+4.11	+3.22	21.3	off-scale	0	0		
97	-6°	+1.471	+5.07	+1.80	19.1	-.98	4.5	1.0	33	
98	-6°	+1.186	+5.63	+1.11	19.1	-.15	20.0	1.5		
99	-6°	+.950	+6.40	+.28	18.3	+.24	23.5	3.0	34 & 35	
100	-6°	2.241	+4.05	+3.25	21.3	off-scale	0	0		
Zero	-6°	-.502	+11.93	+2.09	21.3	.61	—	—		

Parabolic Circular Arc Hydrofoil
#A Cut-off
Reruns

2-13-64
SB-2W

U = 20 FPS

Run No	α	D_{ind}	N_{1ind}	N_{2ind}	P_b psig	P_c Ft H_2O	Q_{ind}	l_c in	Picture No	Remark
Zero	0°	-.482	+11.37	+2.64	21.3	.595	—	—		
Rerun										
101	0°	+1.682	+10.20	+10.45	21.3	off scale	0	0		
102	0°	+.928	+11.97	+8.51	19.5	-.54	5.5	1.0		2.218
103	0°	+.751	+12.52	+8.16	18.6	-.11	20.0	1.5		
104	0°	+.329	+12.52	+6.18	18.7	+.45	27.5	7.0		
105	0°	1.736	+10.18	+10.59	21.3	off scale	0	0		
Zero	0°	-.482	+11.35	+2.63	21.3	.595	—	—		
Zero	+2°	-.480	+11.17	+2.83	21.3	.595	—	—		
106	+2°	+1.816	+13.32	+11.77	21.3	off scale	0	0		
107	+2°	+.819	+15.57	+9.26	19.1	-.151	6.0	1.0		
108	+2°	+.740	+15.86	+9.06	19.3	-.13	11.0	1.5		
109	+2°	1.837	+13.33	11.83	21.3	off scale	0	0		
Zero	+2°	-.478	+11.15	+2.80	21.3	off scale	—	—		

Parabola Circular Arc Hydrofoil
#1 Cut-off

Feb 15, 63
23
J.B. & S.W.

Run No.	α	D_{ind}	$N_{1\,ind}$	$N_{2\,ind}$	P_b	p_e	Q_{ind} lbs	L_e in	Pict No.	Remarks
Batt volt		3.962	3.710	3.731						
Zero	+2°	-.471	11.06	+2.52	21.7	.61	—	—		Floats w/ with st. float
110	+2°	+.348	+18.32	+9.54	21.3	.605	0	0		
111	+2°	+.176	+18.55	+8.85	19.1	+1.24	1.0	.5	36	
112	+2°	+.362	+18.21	+9.57	21.3	.605	0	0		
			11.05							
Zero	+2°	-.480	+11.04	+2.52	21.7	.61	—	—		
crun										Floats w/ with RL. float.
Zero	+2°	-.473	+11.04	+2.54	22.1	.605	—	—		
113	+2°	+.353	+18.29	+9.47	22.0	.75	0	0		w/ RL
114	+2°	+.212	+18.64	+8.96	19.0	1.16	15.5	.125		
115	+2°	+.183	+18.61	+8.85	18.6	1.21	22.0	.150	37	
116	+2	+.157	+18.62	+8.75	18.5	1.26	38.0	.75		
117	+2°	+.385	19.27	+9.60	22.5	.75	0	0		
		-.468	11.03	2.54						
Zero	+2°	-.462	+11.02	+2.55	22.1	.605	—	—		
Battery Voltage		3.962	3.706	3.735						
Battery voltage	2-14-62	3.949	3.590	3.739						
Zero	+4°	-.395	+12.67	+2.77	23.6	.568	—	—		Tow H2O 22.0°C
118	+4°	+.413	+26.06	+10.13	23.6	+.725	0	0		
119	+4°	+.424	+26.08	+10.07	19.7	.955	-2.0	Partly ventilated		
120	+4°	+.395	+26.15	+9.98	19.5	1.00	4.0	2.5	38	mistake wet near strut
121	+4°	+.772	+14.59	+5.71	18.9	+.330	86.0	Devt. losses near stall 10.0	39	
122	+4°	+.615	26.09	10.40	23.2	+.740	0	0		
			12.66	2.77						
Zero	+4°	-.405	+12.65	+2.78	23.6	.568	—	—		

Parabola Circular Arc Hydrofoil 2-14-62
#1 Cut-OFF
24
J.B. + L.W.

U = 20 FPS

Run No	α	D_{ind}	N_{ind}	N_{used}	P_b psig	P_c ft H2O	Q_{ind}	l_c in	Position of Vent	Remarks
Zero	+6°	-.408	+12.42	+2.99	23.6	.568	—	—		
123	+6°	+.597	+32.25	+10.00	24.2	.76	0	0		
124	+6°	+.606	+32.31	+10.09	24.2	.76	0	0		
		unstable vent, near chord, violent probe vibr.								
Zero	+6°	-.405	+12.42	+3.01	23.6	.568	—	—		
Zero	0°	-.392	+13.09	+2.33	23.3	.572	—	—		
125	0°	+.437	+15.91	+7.67	23.0	.640	0	0		
126	0°	+.289	+16.29	+7.30	19.4	.815	2.5	≈.25	40	
27	0°	+.241	+16.37	+7.12	19.3	.955	14.7	≈.50		
128	0°	+.221	+16.21	+7.00	19.4	1.040	31.0	≈.75		
129	0°	+.207	+16.33	+6.92	19.2	1.080	42.0	≈.75		
130	0°	+.175	+16.42	+6.82	19.0	1.150	56.5	≈1.00		
131	0°	+.157	+16.42	+6.74	18.4	1.190	83.5	≈1.00		
132	0°	+.142	+16.37	+6.67	17.7	1.190	109.0	≈1.00		
133	0°	+.454	+15.84	+7.81	22.1	.800	0	0		
		30°	13.07	2.33		572				
Zero	0°	-.403	+13.06	+2.32	23.3	.572	—	—		
Zero	-2°	-.405	+13.30	+2.10	23.3	.572	—	—		
134	-2°	+.570	+12.18	+5.39	23.6	1.080	0	0		
135	-2°	+.401	+12.56	+4.91	19.6	1.035	1.0	≈.25		not complete vent.
136	-2°	+.375	+12.65	+4.81	19.1	1.100	5.5	≈.25		
137	-2°	+.345	+12.75	+4.74	19.2	1.165	17.5	≈.50	41	
138	-2°	+.334	+12.82	+4.62	19.2	1.205	36.5	≈.75		
139	-2°	+.300	+12.84	+4.56	19.2	1.230	57.0	≈.75		
140	-2°	+.277	+12.86	+4.45	18.4	1.255	96.0	≈1.00		
141	-2°	+.616	+12.21	+5.51	22.6	1.090	0	0		
		399	13.29	2.10						
Zero	-2°	-.393	+13.28	2.11	23.3	.572	—	—		

Parabola Circular Arc Hydrofoil
#1 Cut OFF

2-19-62
D.B+L.W. 25

Run no.	α	D_{ind}	W_{ind}	N_{ind}	P_b psig	P_c in H_2O	Q_{ind}	l_c in	Photo no.	Remarks
Zero	$-4°$	-.395	+13.52	+1.88	23.2	.565	—	—		
142	$-4°$	+.792	+9.50	+2.62	22.6	.570	0	0		
143	$-4°$	+.592	+10.01	+2.14	19.8	1.050	3.5	.25		
144	$-4°$	+.575	+10.08	+2.13	19.0	1.100	14.5	.50	42	
145	$-4°$	+.580	+10.12	+2.13	18.3	1.150	43.5	.75		
146	$-4°$	+.817	+9.46	+2.61	22.6	.570	0	0		
Zero	$-4°$	-.391	+13.50	+1.89	23.2	.565	—	—		
Zero	$-6°$	-.389	+13.74 13.78	+1.65	23.2	.565	—	—		
147	$-6°$	+1.162	+7.24	-1.22	23.1	.820	0	0		
148	$-6°$	+.971	+7.68	-1.73	19.6	1.00	3.5	.25		
149	$-6°$	+.902	+7.92	-1.88	18.6	1.150	18.5	.50	43	
150	$-6°$	+.874	+7.98	-1.81	19.0	1.180	28.0	.75		
151	$-6°$	+.849	+8.09	-1.86	19.0	1.230	60.0	.75	44	
152	$-6°$	1.172 387	+7.18	-1.22	22.6	.830	0	0		
Zero	$-6°$	-.385	+13.72	+1.66	23.2	.565	—	—		

Additional Test Data per Jan 25, 26.

#4 cut-off V = 20 fps

JB + L.W.
FSWT.

Run No	α	D_{ind}	$N_{1\,ind}$	$N_{2\,ind}$	p_b psig	p_c psf	q_{ind} mm st. st. float	l_c in	Remarks
8 B	0	+1.193	+1.16	+8.28	19.3	−.47	1.5	.8	h_{ref} = 8.8 ind
9 B	"	1.055	1.57	7.80	19.15	−.22	9.5	1.0	
10 B	"	.851	2.01	7.35	19.15	−.03	20.0	1.5	clear entry at q = 27 mm
11 B	"	.459	2.24	5.73	19.0	+.48	28.5	5-6	
12 B	"	.438	2.34	5.54	18.0	+.51	31.5	6-8	
2910	"	−.360	+.70	1.81	—	+.607	—		
15 B	−6	2.647	−8.44	3.78					
16 B	−4	2.442	−6.64	6.72					h_{ref} = 8.8 in
17 B	−2	2.266	−4.28	9.01					
18 B	0	2.831	−1.79	11.03	fully wetted				
19 B	+2	3.367	+1.74	12.10					
20 B	+4	2.241	+6.17	12.03					
21 B	+6	3.261	11.07	11.41					
2910	−6	−3.14	+1.17	1.22					
"	−4	−3.24	+1.00	1.39					
"	−2	−3.34	+.82	1.58					
"	0	−3.10	+.64	1.78					
"	+2	−3.07	+.46	1.96					
"	+4	−3.02	+.27	2.15					
"	+6	−2.99	+.08	2.34					

NACA 16-006 Strut in 2 Dim. Test Section J.B. & S.W.

$C_D = \frac{D}{\frac{1}{2}\rho U^2 c} = .0139 \frac{D}{h}$

U = 20 FPS

Run No	α	Dwind	Nwind	Wwind	hwind	hfst	Dcorr lbs	C_D	h/c	
Zero	+6°	-.508	+13.53	+3.67	.328					
Zero	+6°	-.508	+13.54	+3.68	.150					
Zero	+6°	-.513	+13.52	+3.69	.500					
Zero	+6°	-.511	+13.50	+3.69	.650					
153	+6°	-.312	+13.06	+4.10	.650	.317	.199	.00865	1.69	href=.967
154	+6°	-.220	+12.99	+4.25	.500	.467	.293	.00865	2.49	
155	+6°	-.117	+12.84	+4.36	.328	.639	.391	.00845	3.40	
156	+6°	+.019	+12.80	+4.51	.150	.817	.489	.00825	4.35	
Zero	+6°	-.500	+13.55	+3.68	.150					
Zero	+6°	-.505	+13.54	+3.69	.500					
Zero	+4°	-.503	+13.59	+3.60	.500					
Zero	+4°	-.500	+13.61	+3.61	.328					
Zero	+4°	-.498	+13.62	+3.62	.150					
157	+4°	-.003	+12.92	+4.37	.150	.819	.495	.00835	4.36	
158	+4°	-.083			.328	.641	.417	.0090	3.42	
159	+4°	-.184			.500	.469	.319	.00940	2.50	
160	+4	-.252			.650	.319	.246	.01064	1.70	href=.969
Zero	+4°	-.498			.500					
Zero	+4°	-.493			.328					
Zero	+2°	-.497			.328					
161	+2°	-.126			.328	.646	.373	.00796	3.44	
162	+2°	-.016			.150	.824	.483	.00810	4.39	
163	+2°	-.215			.500	.474	.284	.00828	2.52	
164	+2°	-.293			.650	.324	.206	.00878	1.72	href .974
Zero		-.502			.650					

NACA 16-006 Strut Drag

2-15-62 JB + L.W.

Run No.	α	Pind	Hind	b ft	D corr lbs	c_D	h/c		
Zero	0°	-.499							
165	0°	-.300	.650	.323	.200	.00855	1.72		h_{REF} .973
166	0°	-.223	.500	.473	.277	.00808	2.52		
167	0°	-.122	.328	.645	.378	.00809	3.44		
168	0°	-.022	.150	.823	.478	.00802	4.39		
Zero	0°	-.505							
Zero	-2°	-.494							h_{REF} .972
169	-2°	-.305	.650	.322	.195	.00837	1.72		
170	-2°	-.223	.500	.472	.277	.00810	2.52		
171	-2°	-.120	.328	.644	.380	.00815	3.44		
172	-2°	-.010	.150	.822	.490	.00823	4.39		
Zero	-2°	-.505							
Zero	-4°	-.503							
173	-4°	-.307	.650	.322	.199	.00854	1.72		h_{REF} .972
174	-4°	-.222	.500	.472	.284	.00830	2.52		
175	-4°	-.123	.328	.644	.383	.00822	3.44		
176	-4°	-.029	.150	.822	.477	.00801	4.39		
Zero	-4°	-.510							
Zero	-6°	-.512							
177	-6°	-.314	.650	.321	.198	.00853	1.71		h_{REF} .971
178	-6°	-.227	.500	.471	.285	.00835	2.51		
179	-6°	-.140	.328	.643	.372	.0080	3.43		
180	-6°	-.030	.150	.821	.482	.00810	4.38		
Zero	-6°	-.512							

NACA 16-006 strut in open channel FSWT.

March 22, '62 29

H_2O max 8.09 ft = 20.2 fps

JB + L.W.

Run No	α ind	D ind	h ind	D corr lbs	Run no	α corr	D ind	h ind	D corr lbs	h corr
Calib.	pan wt	+.320	check.		Zero	-2°	-.056	.819		
	1 lbs	+1.315			197	-2°	+.020	.690	.076	.139
	pan wt	+.319			198	-2°	+.115	.500	.171	.319
Zero	0	-.064	.818		199	-2°	+.213	.330	.269	.489
181	0	+.022	.690	.087	200	-2°	+.325	.150	.381	.669
182	0	+.116	.500	.181	Zero	-2°	-.057			
183	0	+.215	.330	.280						
184	0	+.307	.150	.372	Zero	-4°	-.056	.818		
Zero	0	-.066			201	-4°	+.027	.690	.081	
					202	-4°	+.121	.500	.175	
Zero	+2	-.067	.819		203	-4°	+.222	.330	.276	
185	+2°	+.019	.690	.082	204	-4°	+.323	.150	.377	
186	+2°	+.116	.500	.179	Zero	-4°	-.053			
187	+2°	+.210	.330	.273						
188	+2°	+.326	.150	.389	Zero	-6°	-.057	.813		
Zero	+2°	-.058			205	-6°	+.021	.690	.079	.123
					206	-6°	+.112	.500	.170	.313
Zero	+4°	-.058	.818		207	-6°	+.217	.330	.275	.483
189	+4°	+.022	.690	.080	208	-6°	+.321	.150	.379	.663
190	+4°	+.122	.500	.180	Zero	-6°	-.060			
191	+4°	+.225	.330	.283						
192	+4°	+.335	.150	.393						
Zero	+4°	-.059								
Zero	+6°	-.054	.819							
193	+6°	+.032	.690	.086						
194	+6°	+.124	.500	.178						
195	+6°	+.216	.330	.270						
196	+6°	+.336	.150	.390						
Zero	+6°	-.055								

Thrust of Air Jet on Foil Base.

3/16/62 30

GB + L.W.

Run No.	Land	Q final cfm at float	P_b psig	D in d	D lbs
Zero	0	0	—	-.087	
209	"	10	14.2	-.088	.001
210	"	33	13.9	-.087	0
211	"	70	13.5	-.090	.003
212	"	110	12.8	-.094	.007

Foil Base Area

#1 c.o. A_b = .858 in^2

#2 c.o. 1.29 in^2

#3 c.o. 1.76 in^2

#4 c.o. 2.11 in^2

TABLE I

MODIFIED PARABOLIC HYDROFOIL PROFILE AND COORDINATES

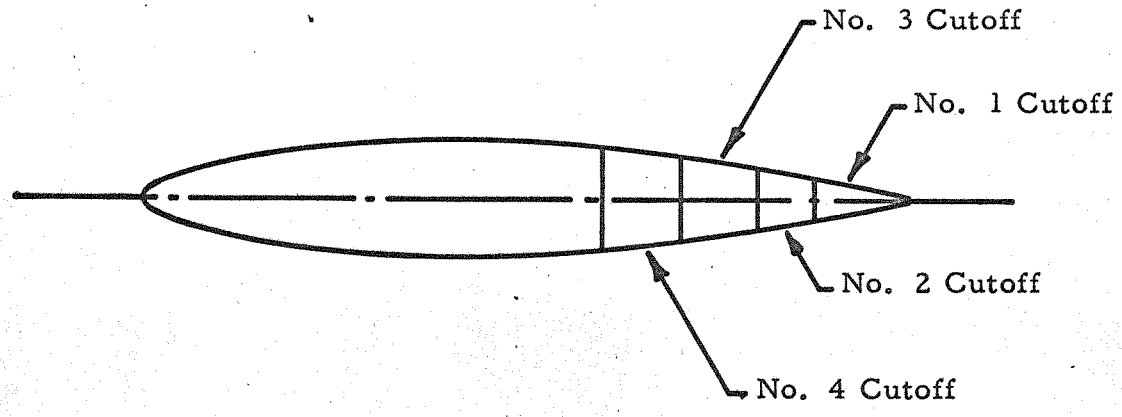

No. 4 Cutoff at x/c = .60
No. 3 Cutoff at x/c = .70
No. 2 Cutoff at x/c = .80
No. 1 Cutoff at x/c = .875

x	y	x	y
.0	.0000	1.6000	.3000
.0200	.0449	1.8000	.2974
.0300	.0550	2.0000	.2902
.0500	.0709	2.2000	.2788
.1000	.1000	2.4000	.2632
.2000	.1404	2.6000	.2436
.3000	.1703	2.8000	.2201
.4000	.1944	3.0000	.1927
.6000	.2316	3.2000	.1616
.8000	.2585	3.4000	.1266
1.0000	.2778	3.6000	.0880
1.2000	.2906	3.8000	.0458
1.4000	.2979	4.0000	.0000

L. E. radius = .044 inches

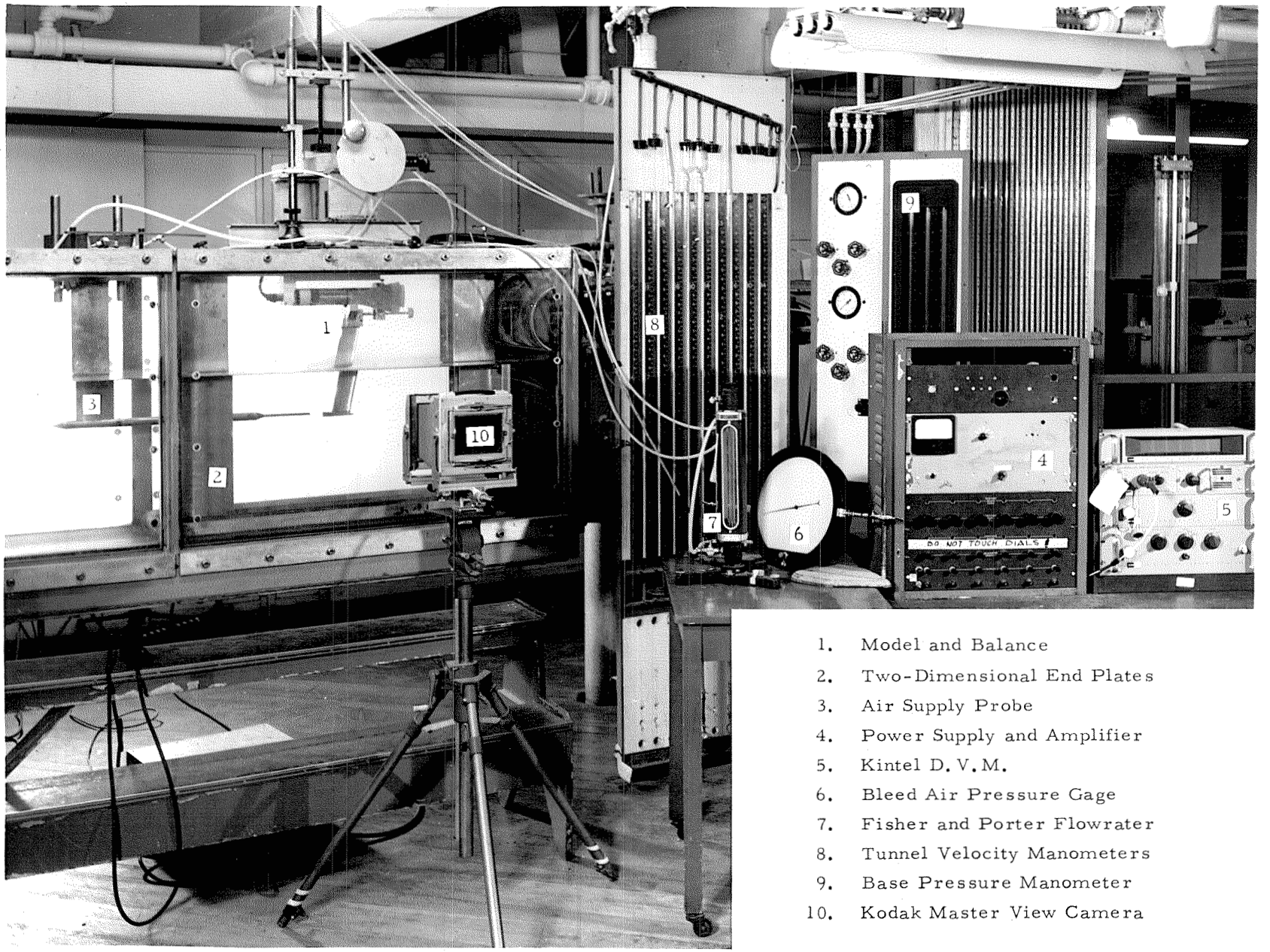

1. Model and Balance
2. Two-Dimensional End Plates
3. Air Supply Probe
4. Power Supply and Amplifier
5. Kintel D. V. M.
6. Bleed Air Pressure Gage
7. Fisher and Porter Flowrater
8. Tunnel Velocity Manometers
9. Base Pressure Manometer
10. Kodak Master View Camera

Fig. 1 Free-Surface Water Tunnel Working Section and Apparatus

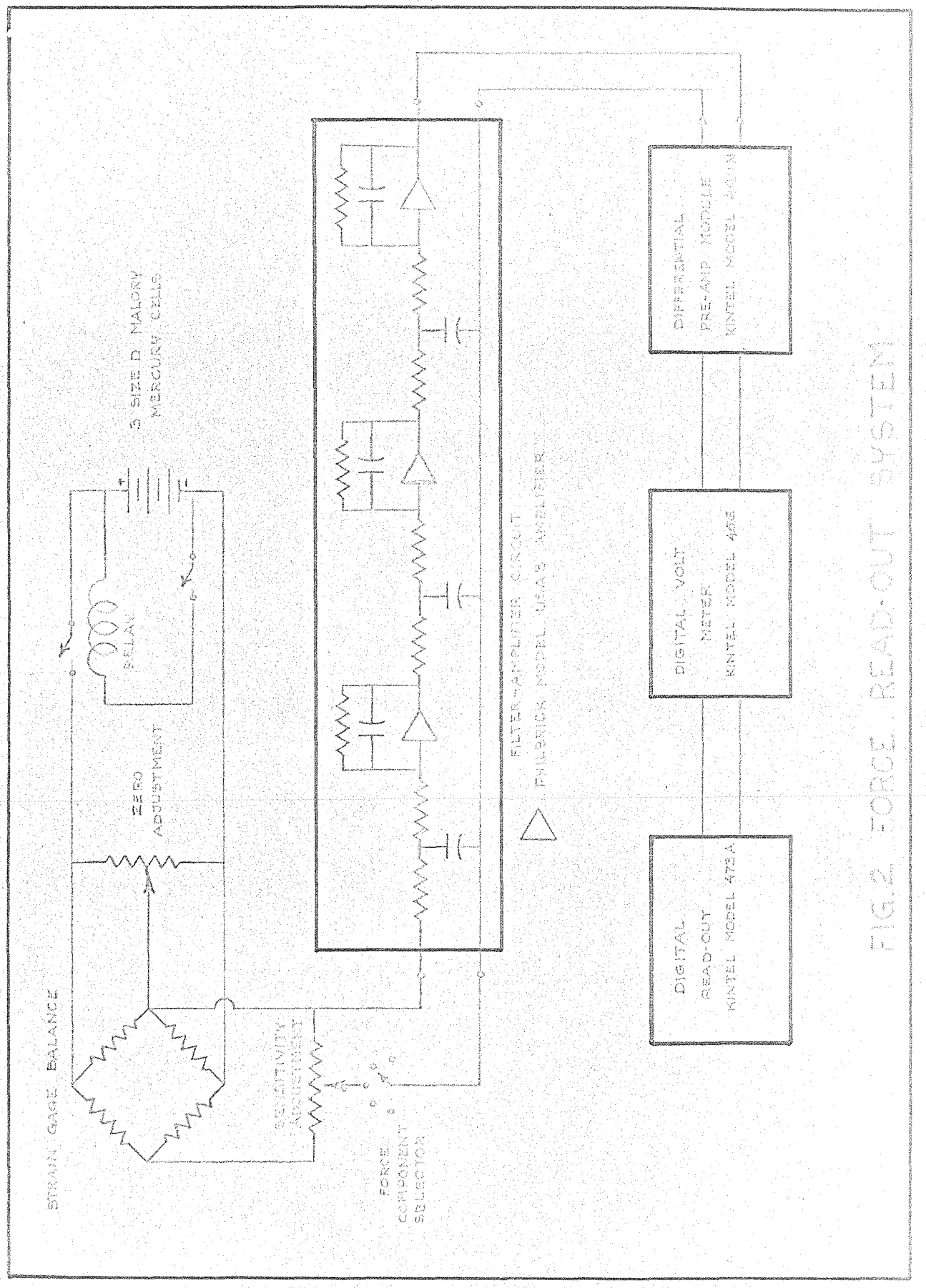

FIG. 2. FORCE READ-OUT SYSTEM

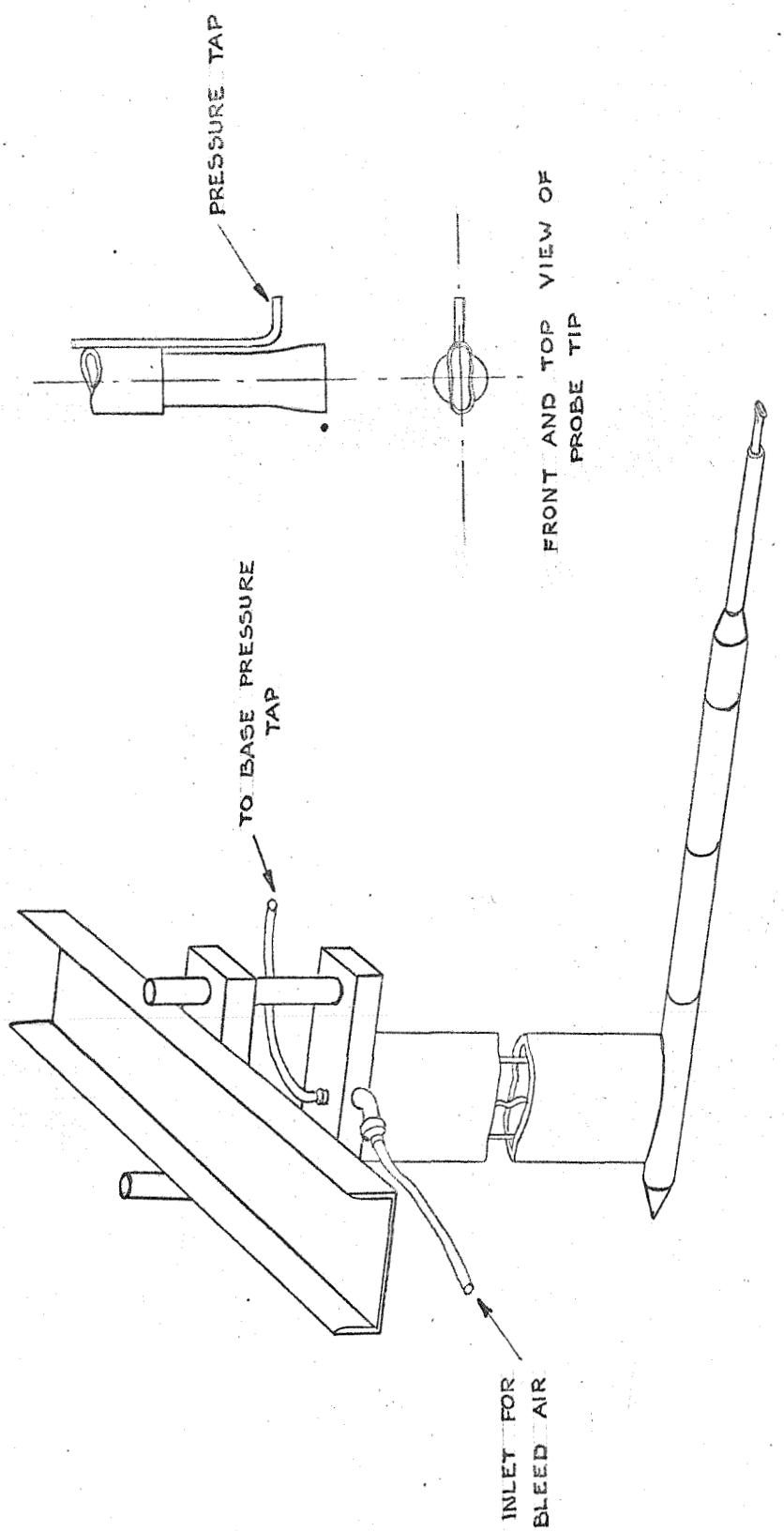

FIG. 3 VENTILATION PROBE

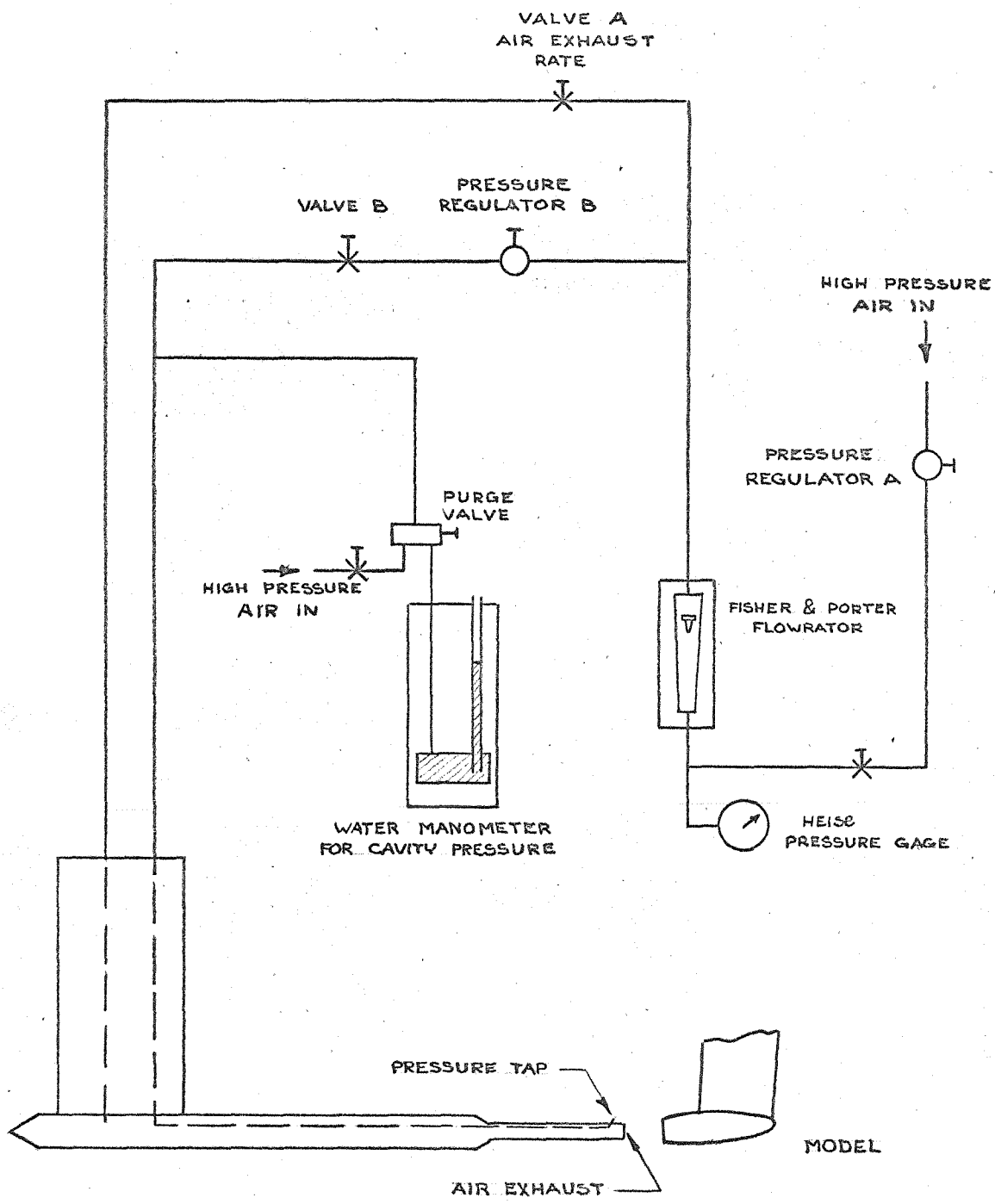

FIG. 4 AIR FLOW DIAGRAM

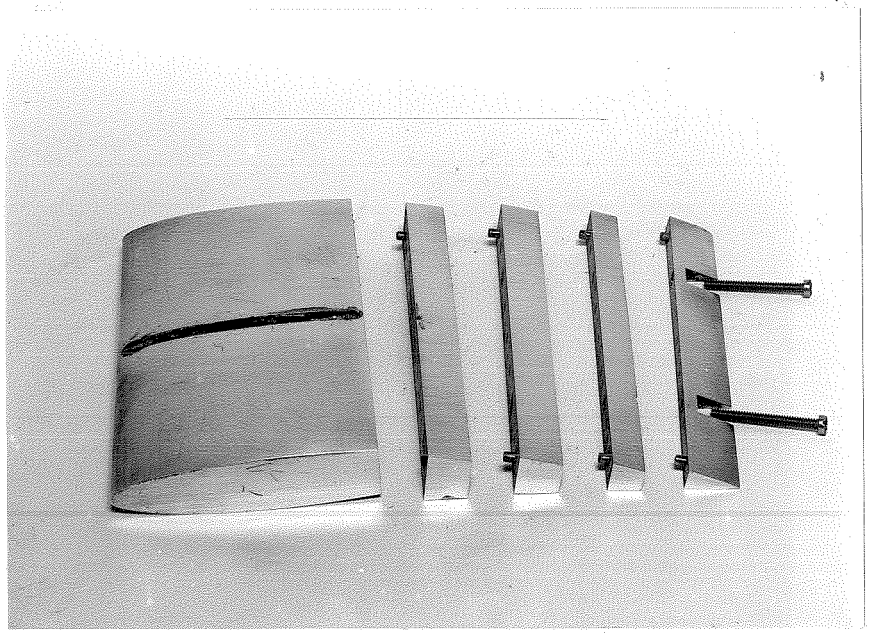

Fig. 5 - Modified Parabola Hydrofoil Model, Showing the Cutoff Trailing Edge Sections, the Dowel Pins, Retaining Screws, and the Slot for the NACA 16-006 Strut

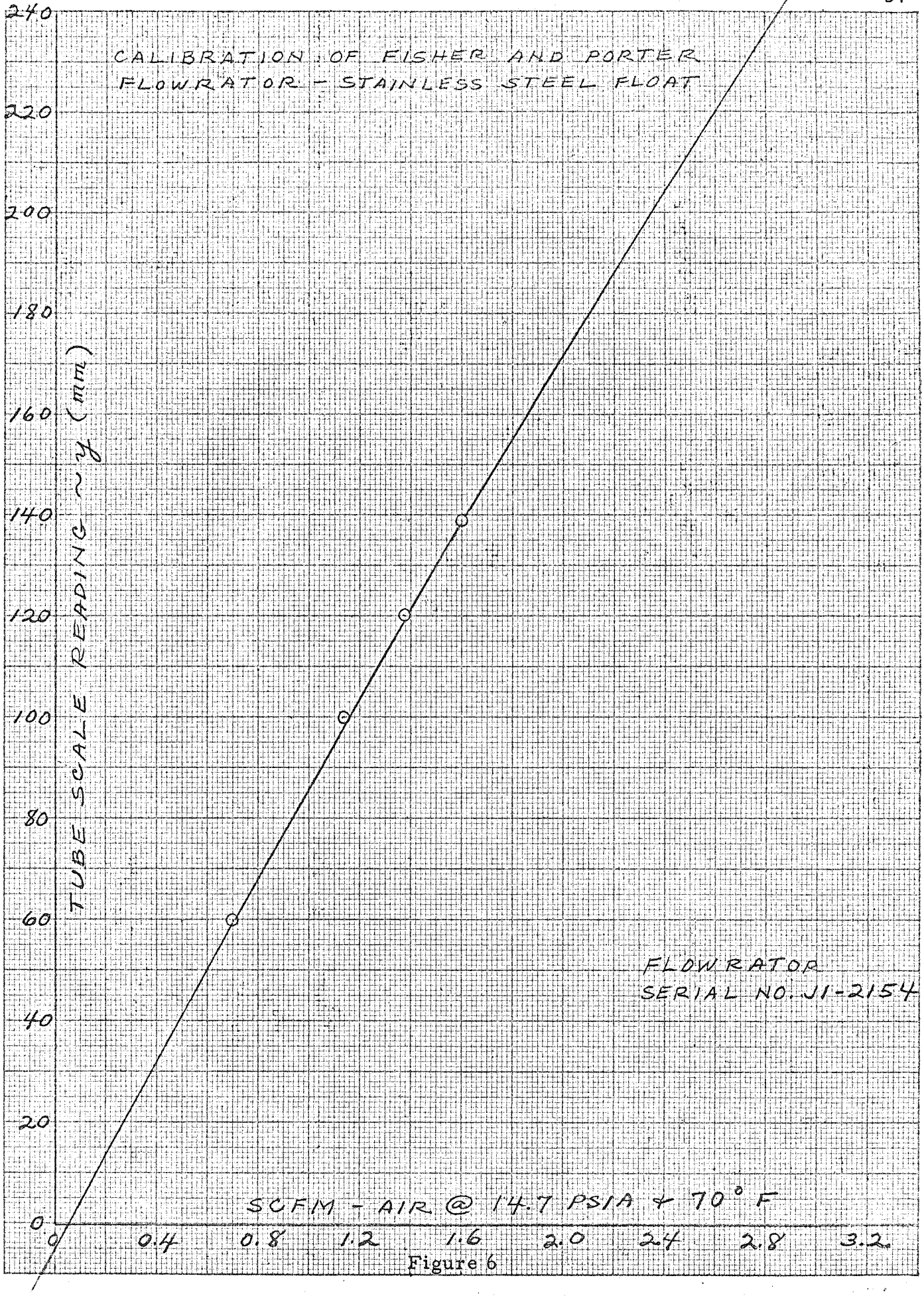
CALIBRATION OF FISHER AND PORTER
FLOWRATOR - STAINLESS STEEL FLOAT
TUBE SCALE READING ~ y (mm)
240
220
200
180
160
140
120
100
80
60
40
20
0
0
0.4
0.8
1.2
1.6
2.0
2.4
2.8
3.2
SCFM - AIR @ 14.7 PSIA + 70° F
FLOWRATOR
SERIAL NO. J1-2154

Figure 6

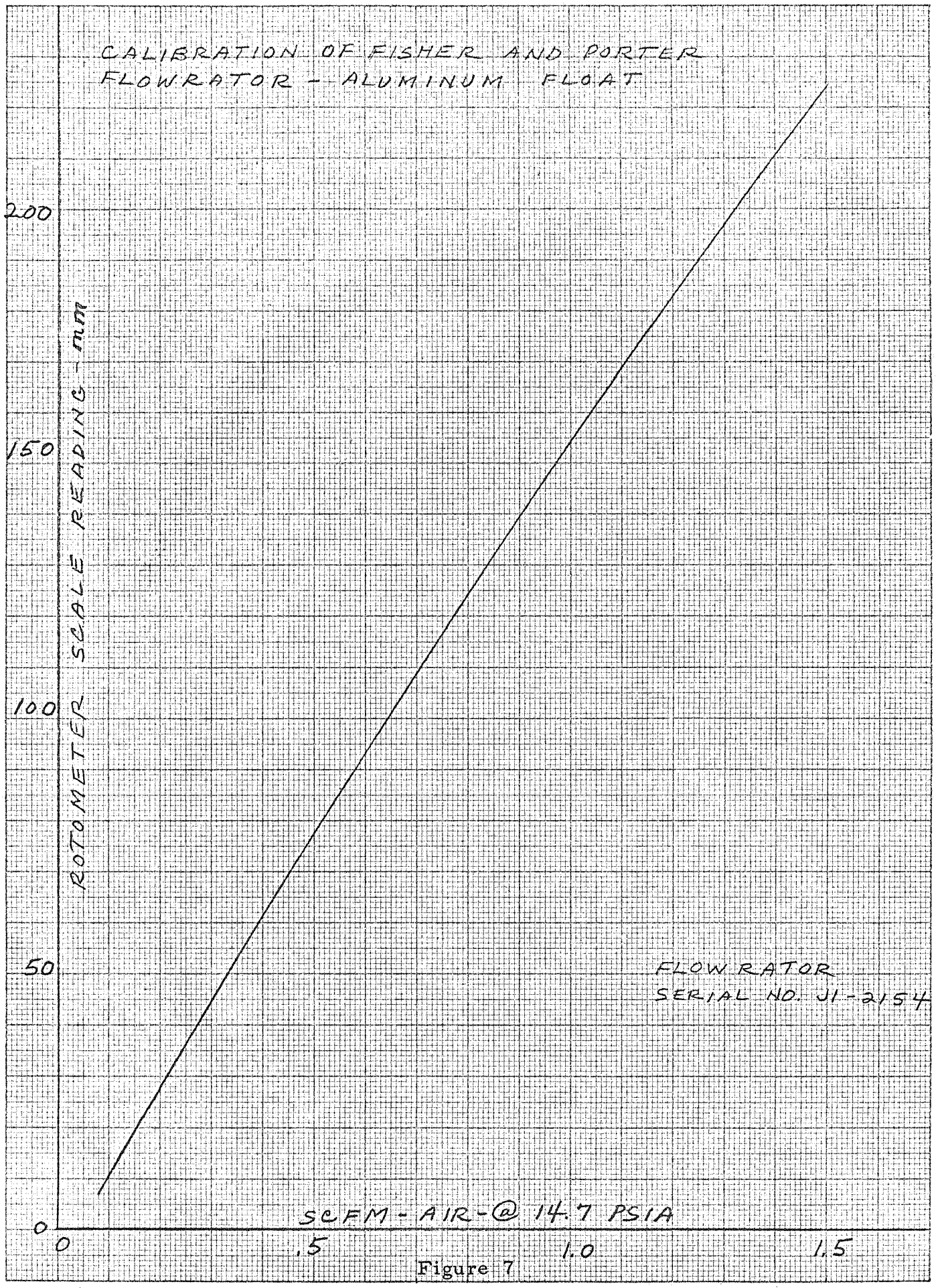
CALIBRATION OF FISHER AND PORTER
FLOWRATOR - ALUMINUM FLOAT
ROTOMETER SCALE READING - mm
200
150
100
50
0
0
.5
1.0
1.5
SCFM - AIR - @ 14.7 PSIA
FLOWRATOR
SERIAL NO. J1-2154

Figure 7

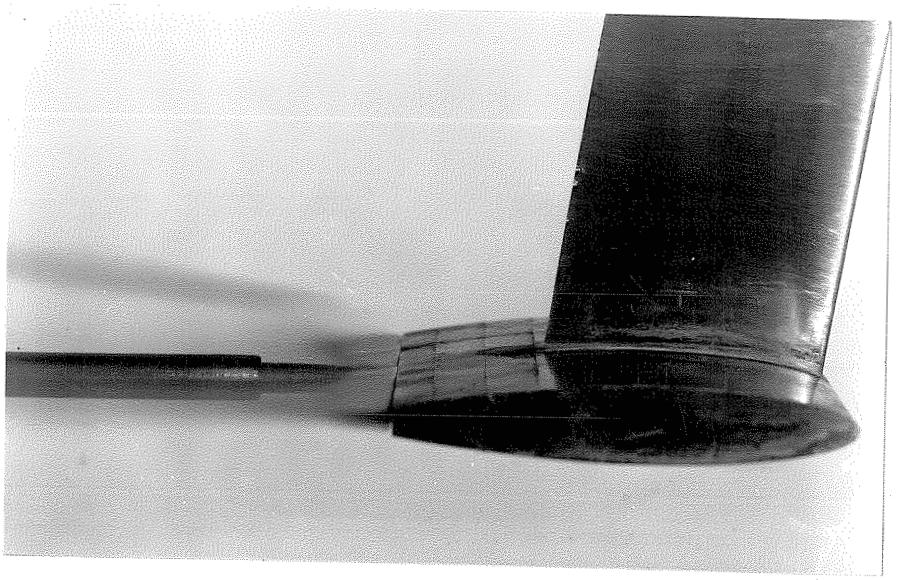

Angle of Attack = 0^{o}; $Q' = .0112$

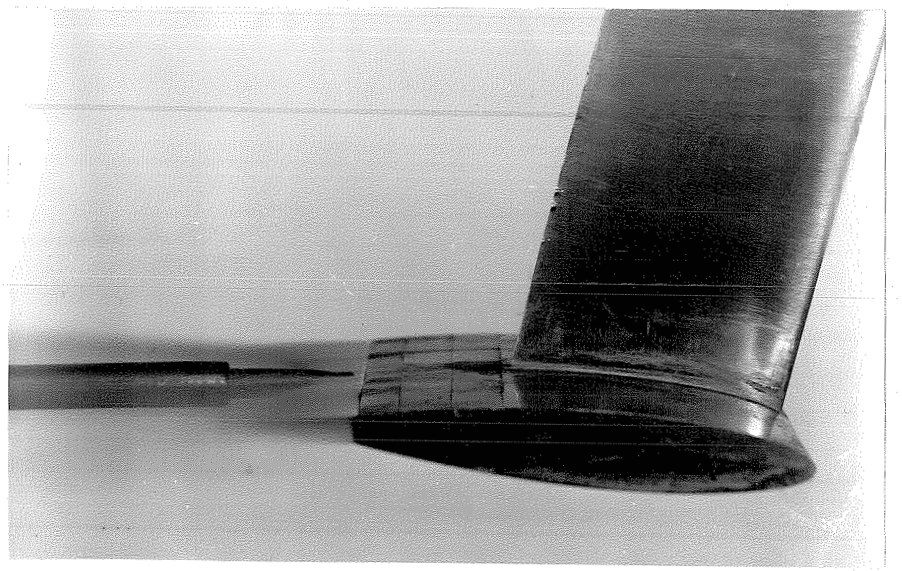

Angle of Attack = -6^{o}; $Q' = .0296$

Fig. 8 - Ventilation of the Number One Cutoff
V = 20 fps

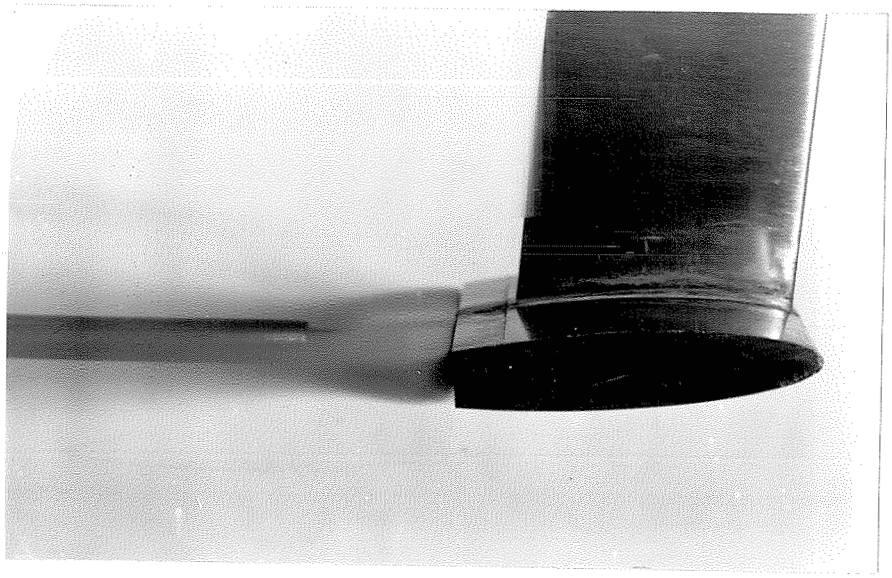

Angle of Attack = $+4^{\circ}$; $Q^{\#} = .0056$

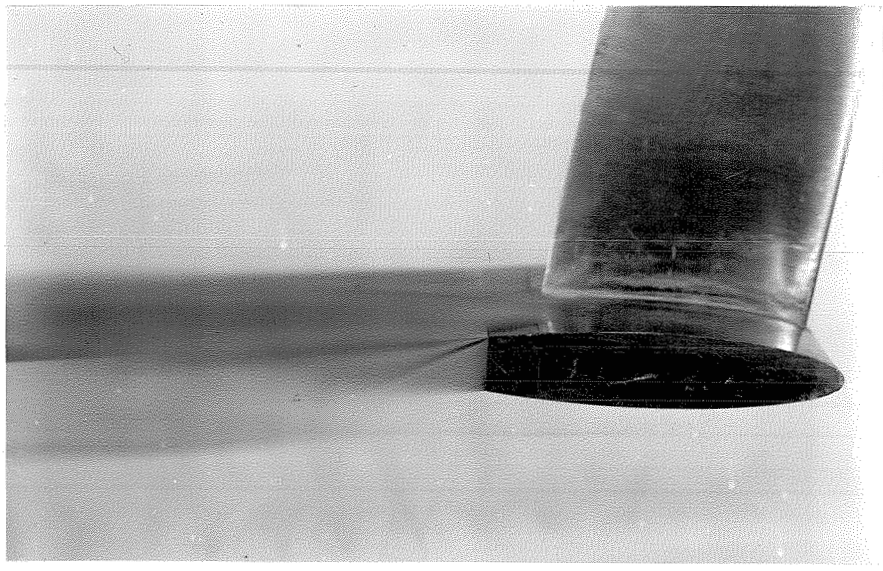

Angle of Attack = -6°; $Q^{\#} = .0417$
Note upper surface ventilation.

Fig. 9 - Ventilation of Number Three Cutoff.
V = 20 fps

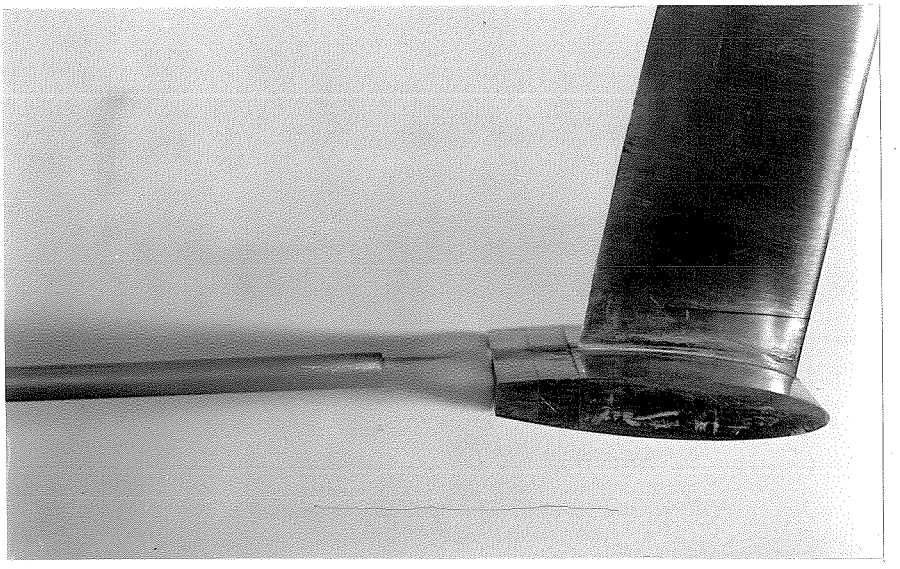

Angle of Attack = -6°; $Q' = .00645$

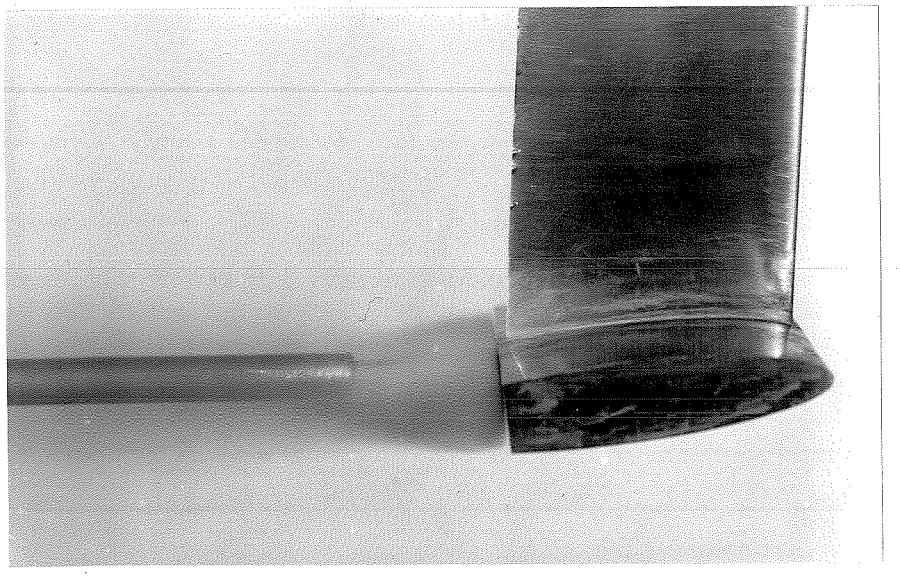

Angle of Attack = $+6^{\circ}$; $Q' = .0069$

Fig. 10 - Ventilation of Numbers Two and Four Cutoffs
V = 20 fps

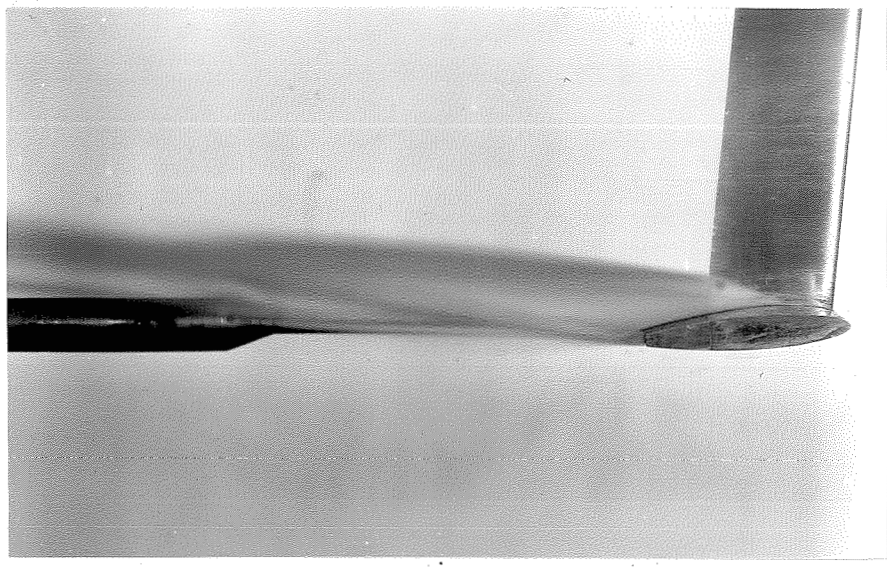

Angle of Attack = + 4°; $Q' = .1183$
V = 20 fps
(Time Exposure)

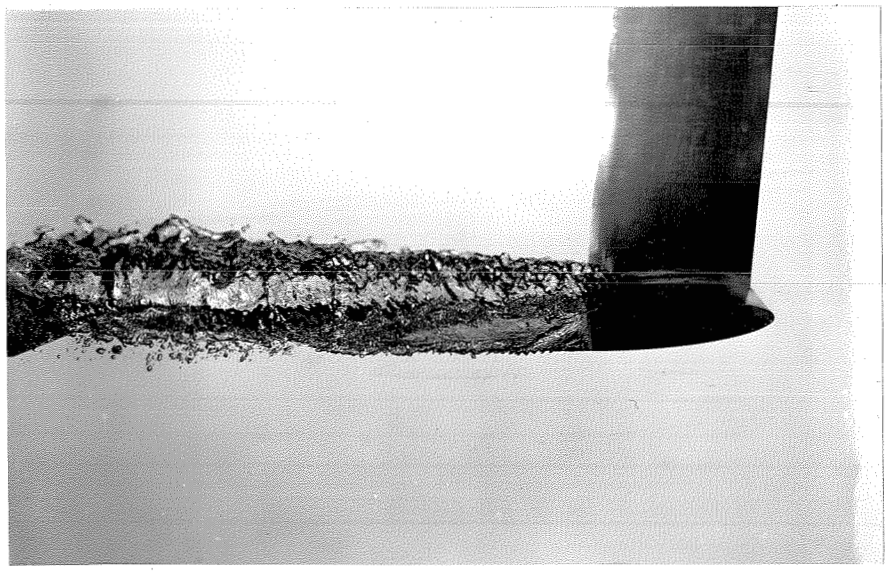

Angle of Attack = +2°; $Q' = .0727$
V = 15 fps
(Electronic Flash Photograph)

Fig. 11 - Ventilation at Foil-Strut Intersection; Number One and Four Cutoffs.

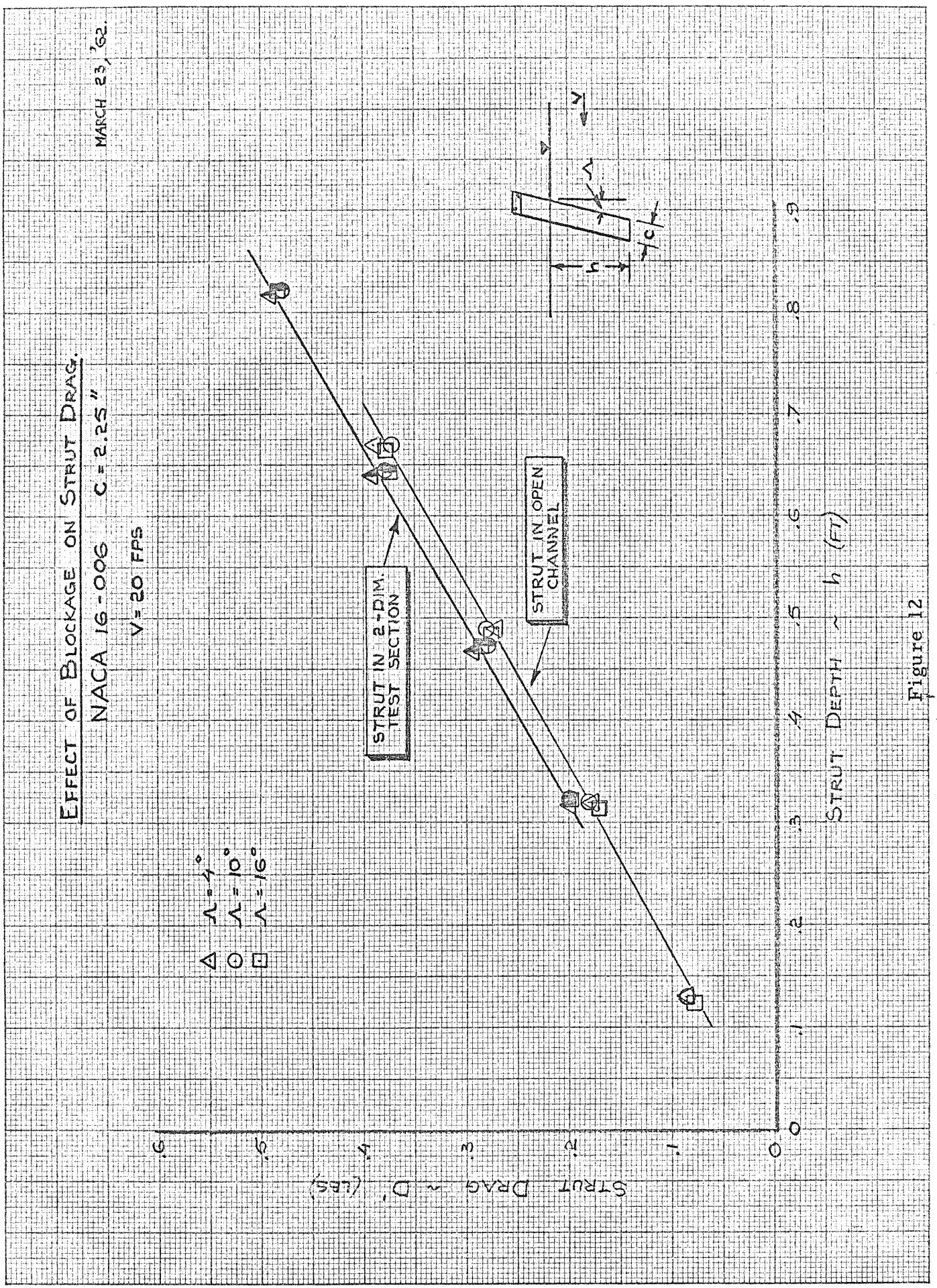
EFFECT OF BLOCKAGE ON STRUT DRAG.
NACA 16-006 C = 2.25"
V = 20 FPS
MARCH 23, '62.
Δ Λ = 4°
○ Λ = 10°
□ Λ = 16°
STRUT IN 2-DIM. TEST SECTION
STRUT IN OPEN CHANNEL
V
Λ
h
h/c
STRUT DRAG ~ D' (LBS)
STRUT DEPTH ~ h (FT)
0
.1
.2
.3
.4
.5
.6
.7
.8
.9
.1
.2
.3
.4
.5
.6

Figure 12

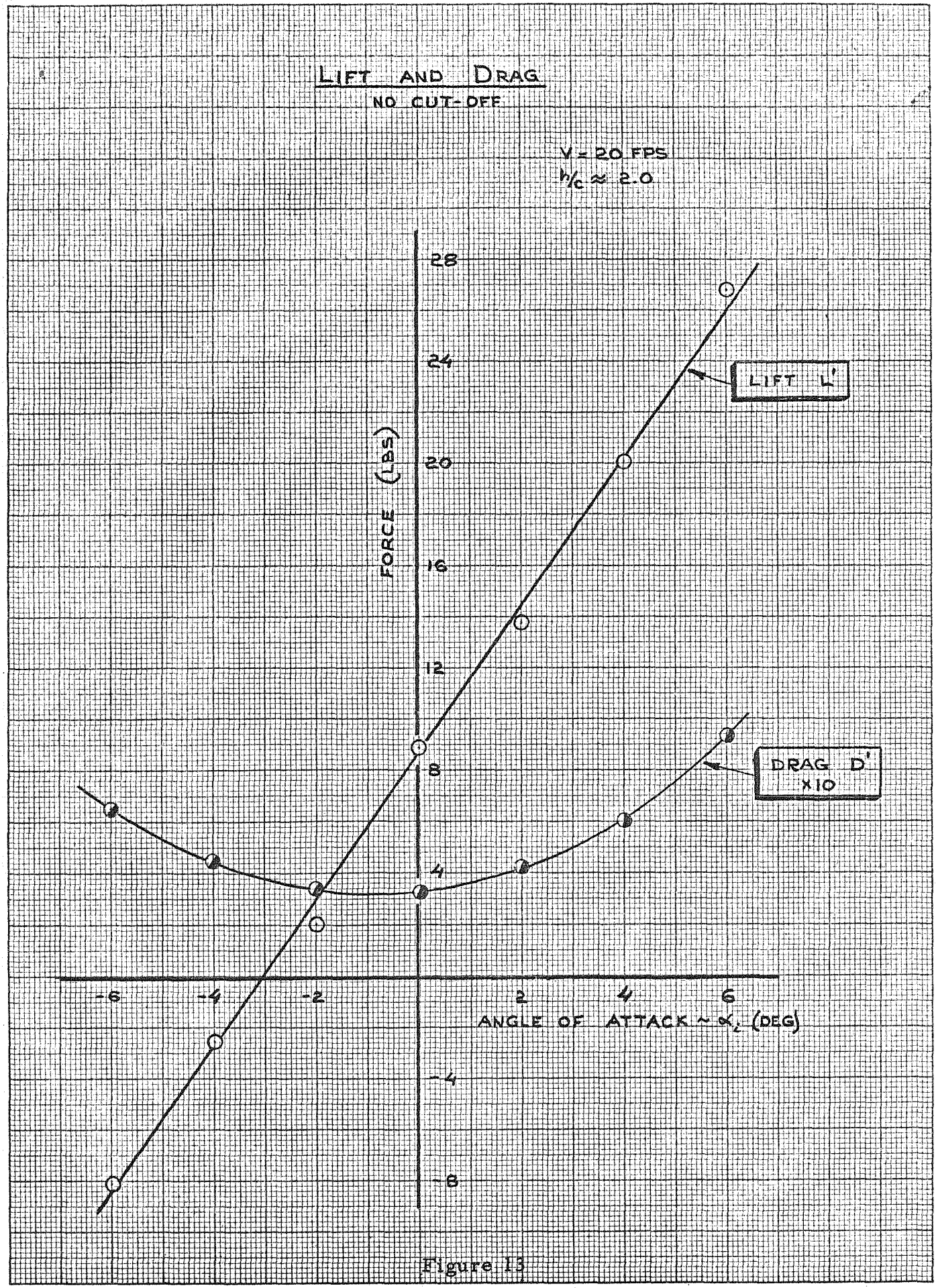
LIFT AND DRAG
NO CUT-OFF
V = 20 FPS
h/c ≈ 2.0
28
24
20
16
12
8
4
-4
-8
FORCE (LBS)
LIFT L'
DRAG D'
X10
-6
-4
-2
2
4
6
ANGLE OF ATTACK ~ α_i (DEG)

Figure 13

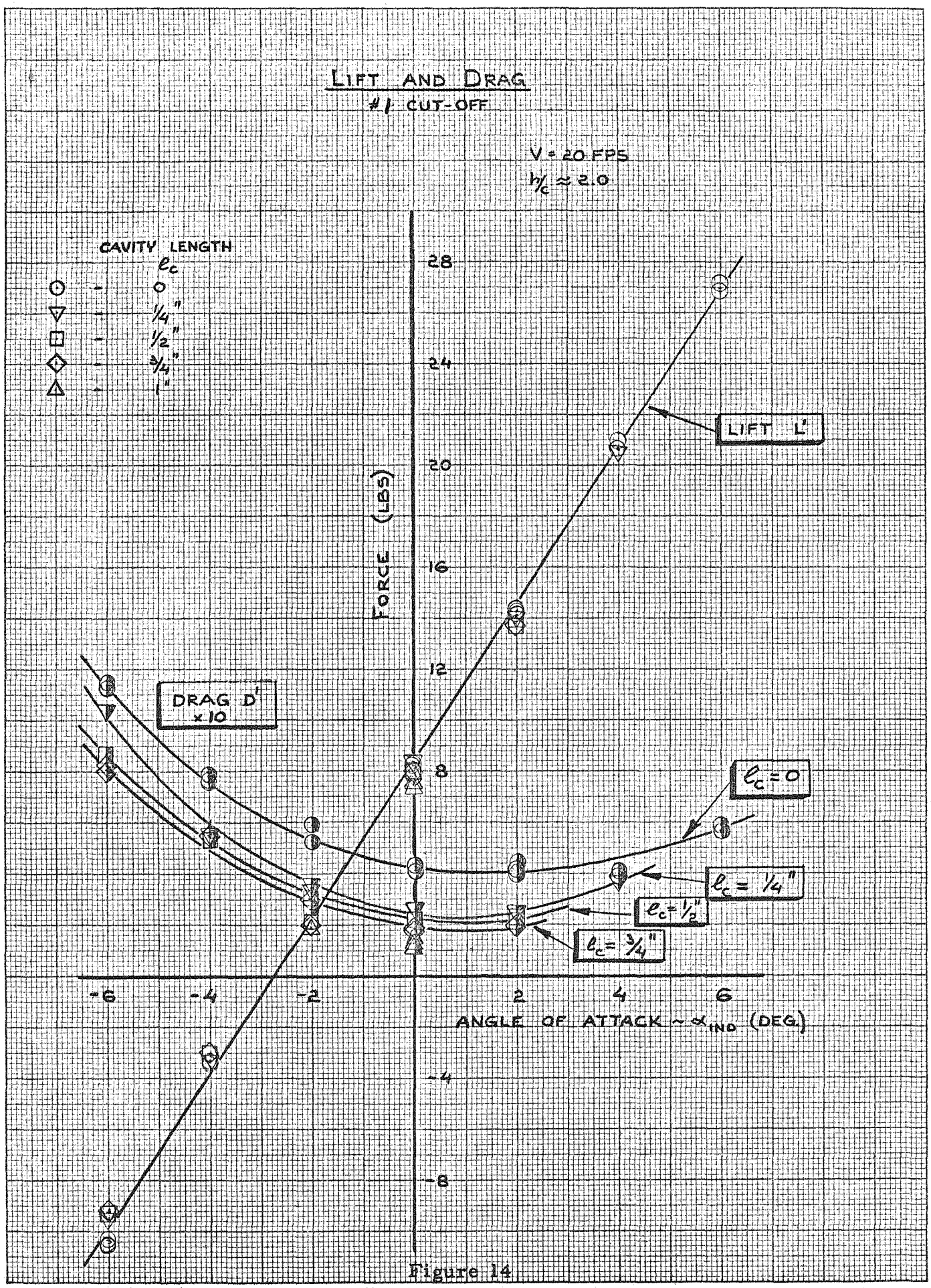
LIFT AND DRAG
#1 CUT-OFF
V = 20 FPS
h/c ≈ 2.0
CAVITY LENGTH
ℓ_c
○ - 0
▽ - 1/4"
□ - 1/2"
◇ - 3/4"
△ - 1"
28
24
20
16
12
8
-4
-8
FORCE (LBS)
LIFT L'
DRAG D'
x10
ℓ_c = 0
ℓ_c = 1/4"
ℓ_c = 1/2"
ℓ_c = 3/4"
-6
-4
-2
2
4
6
ANGLE OF ATTACK ~ α_{IND} (DEG.)

Figure 14

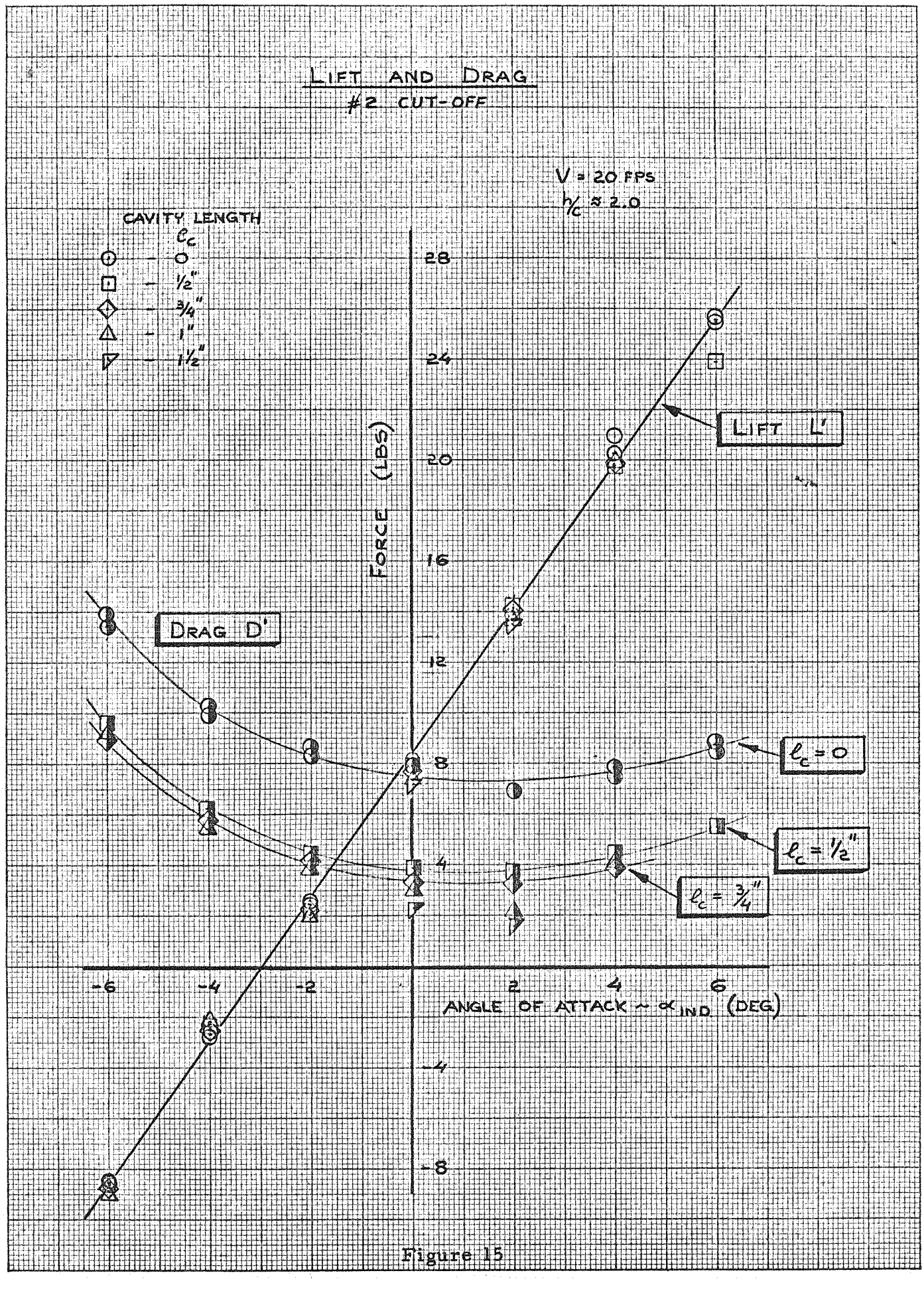
LIFT AND DRAG
#2 CUT-OFF
V = 20 FPS
h/c ≈ 2.0
CAVITY LENGTH
ℓ_c
○ – 0
□ – 1/2"
◇ – 3/4"
△ – 1"
▽ – 1 1/2"
LIFT L'
DRAG D'
ℓ_c = 0
ℓ_c = 1/2"
ℓ_c = 3/4"
FORCE (LBS)
28
24
20
16
12
8
4
-4
-8
-6
-4
-2
2
4
6
ANGLE OF ATTACK ~ $\alpha_{IND.}$ (DEG.)

Figure 15

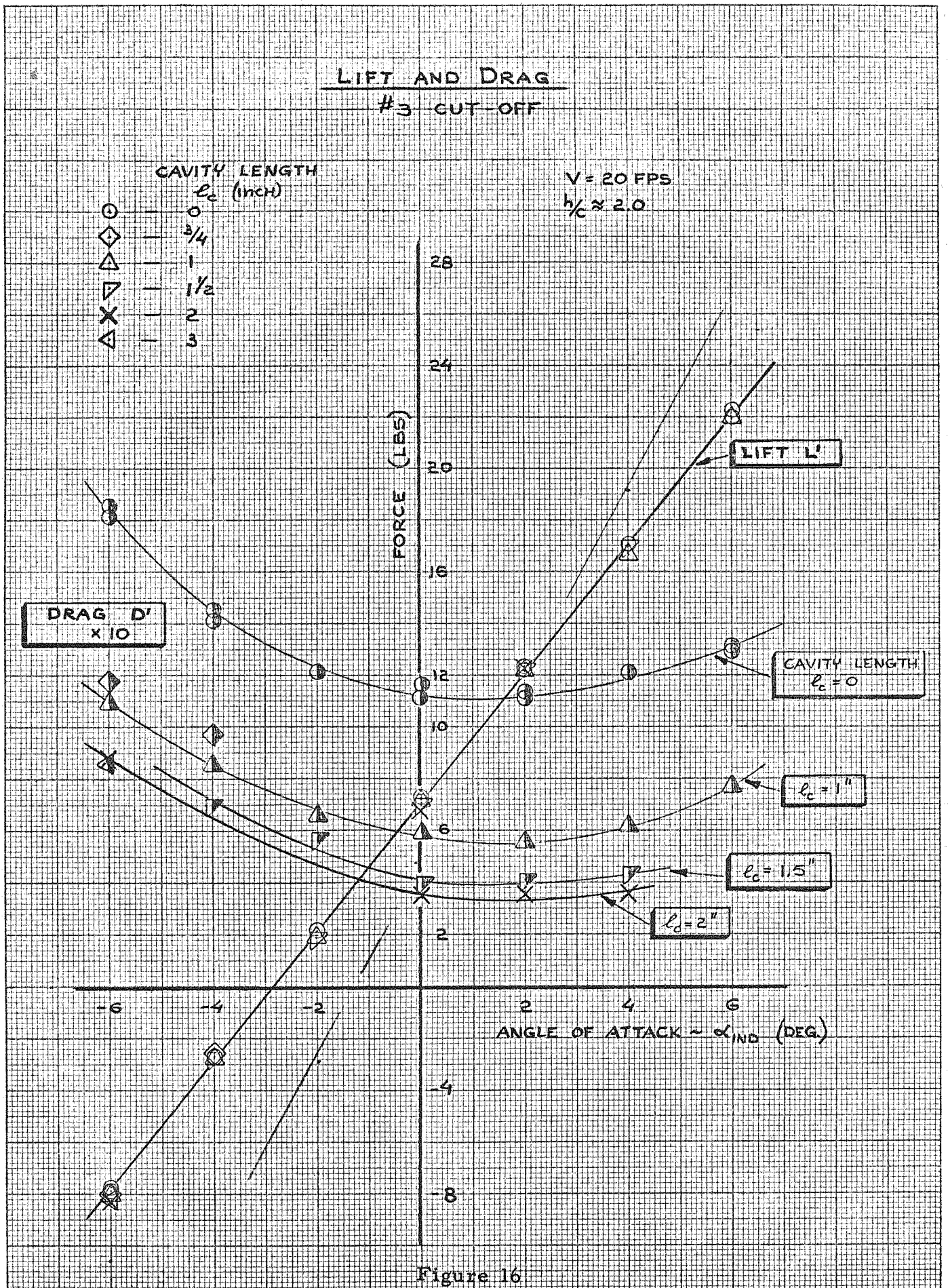
LIFT AND DRAG
#3 CUT-OFF
CAVITY LENGTH
ℓ_c (inch)
0
3/4
1
1 1/2
2
3
V = 20 FPS
$h/c \approx 2.0$
28
24
20
16
12
10
6
2
-4
-8
FORCE (LBS)
LIFT L'
DRAG D'
x 10
CAVITY LENGTH
$\ell_c = 0$
$\ell_c = 1"$
$\ell_c = 1.5"$
$\ell_c = 2"$
-6
-4
-2
2
4
6
ANGLE OF ATTACK ~ α_{IND} (DEG.)

Figure 16

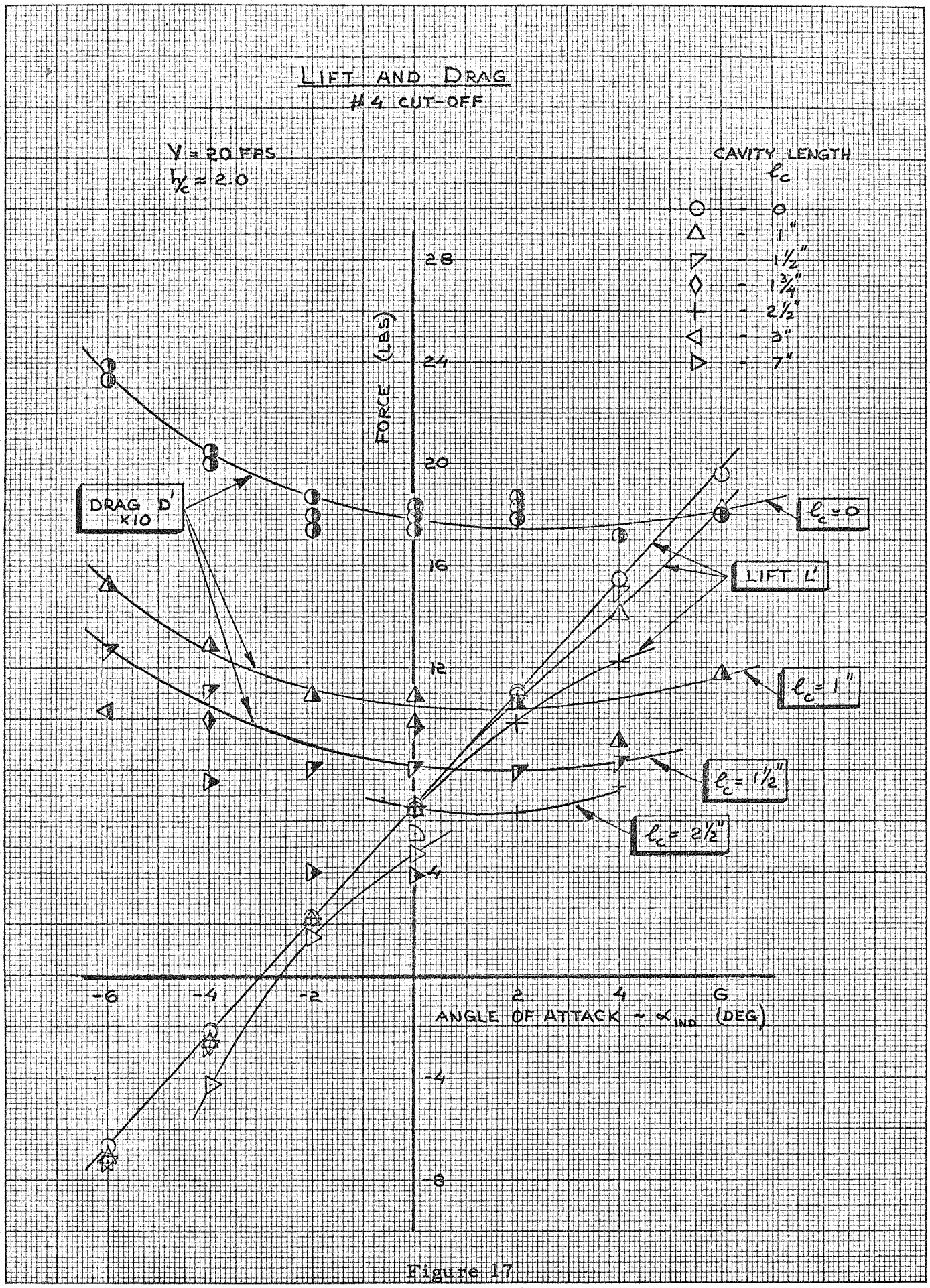
LIFT AND DRAG
#4 CUT-OFF
V = 20 FPS
h/c = 2.0
CAVITY LENGTH
ℓ_c
○ - 0
△ - 1"
▽ - 1½"
◇ - 1¾"
+ - 2½"
◁ - 3"
▷ - 7"
FORCE (LBS)
28
24
20
16
12
8
4
-4
-8
DRAG D'
x10
LIFT L'
ℓ_c=0
ℓ_c= 1"
ℓ_c= 1½"
ℓ_c= 2½"
-6
-4
-2
2
4
6
ANGLE OF ATTACK ~ $\alpha_{IND.}$ (DEG)

Figure 17

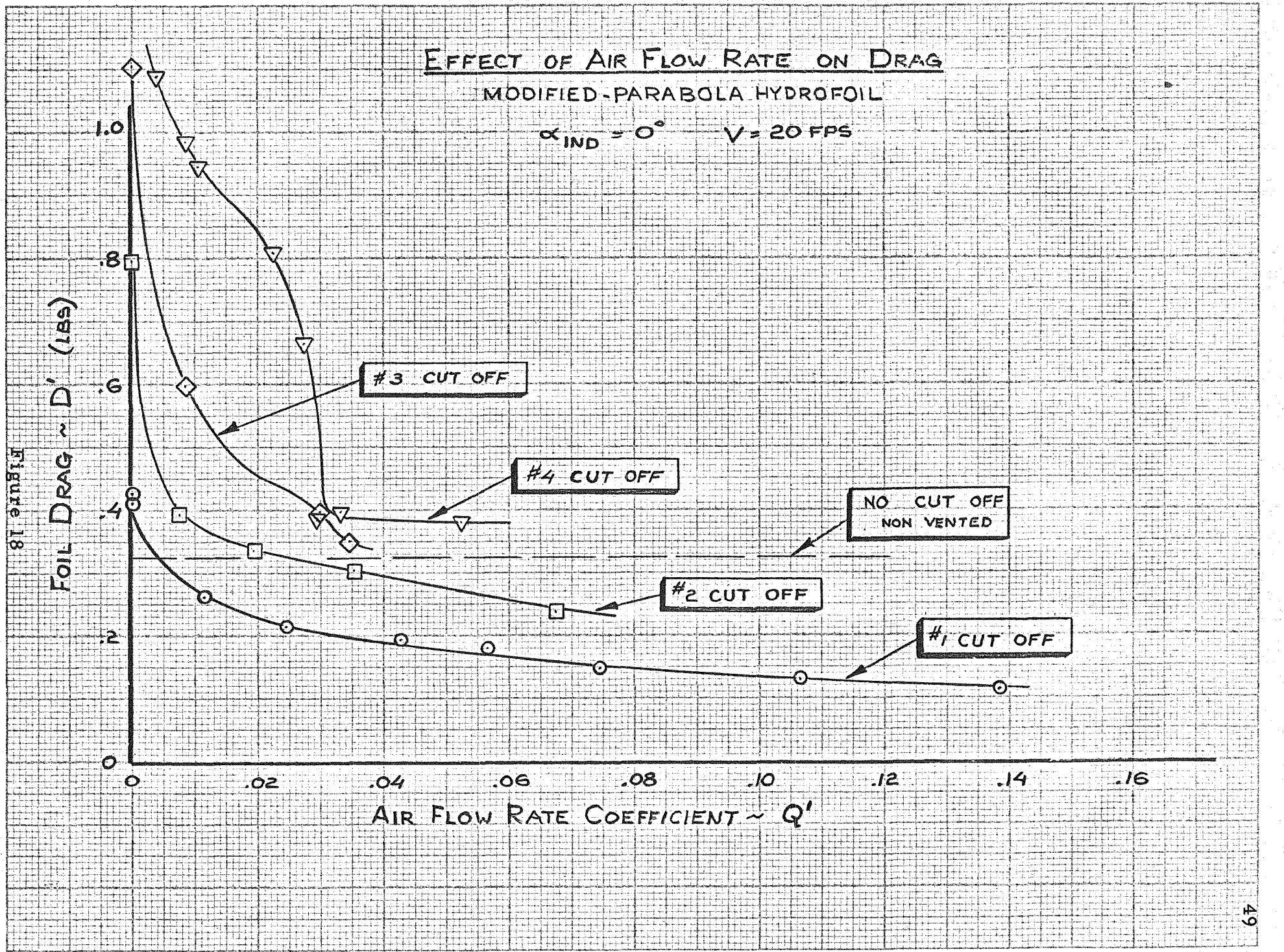

Figure 18

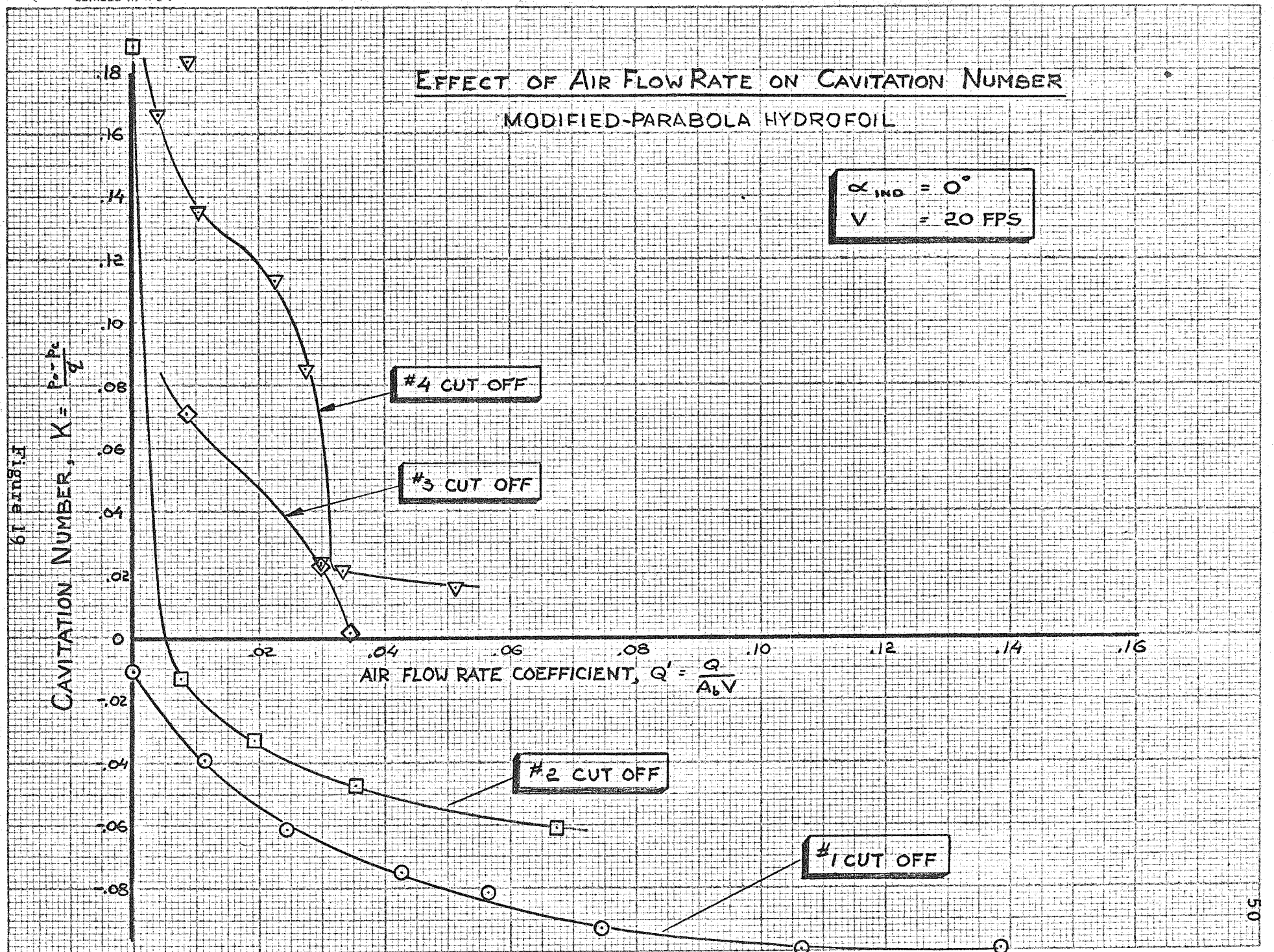
EFFECT OF AIR FLOW RATE ON CAVITATION NUMBER
MODIFIED-PARABOLA HYDROFOIL
$\alpha_{IND} = 0°$
V = 20 FPS
#4 CUT OFF
#3 CUT OFF
#2 CUT OFF
#1 CUT OFF
CAVITATION NUMBER, $K = \frac{P_o - P_c}{q}$
AIR FLOW RATE COEFFICIENT, $Q' = \frac{Q}{A_b V}$
.18
.16
.14
.12
.10
.08
.06
.04
.02
0
-.02
-.04
-.06
-.08
.02
.04
.06
.08
.10
.12
.14
.16

Figure 19

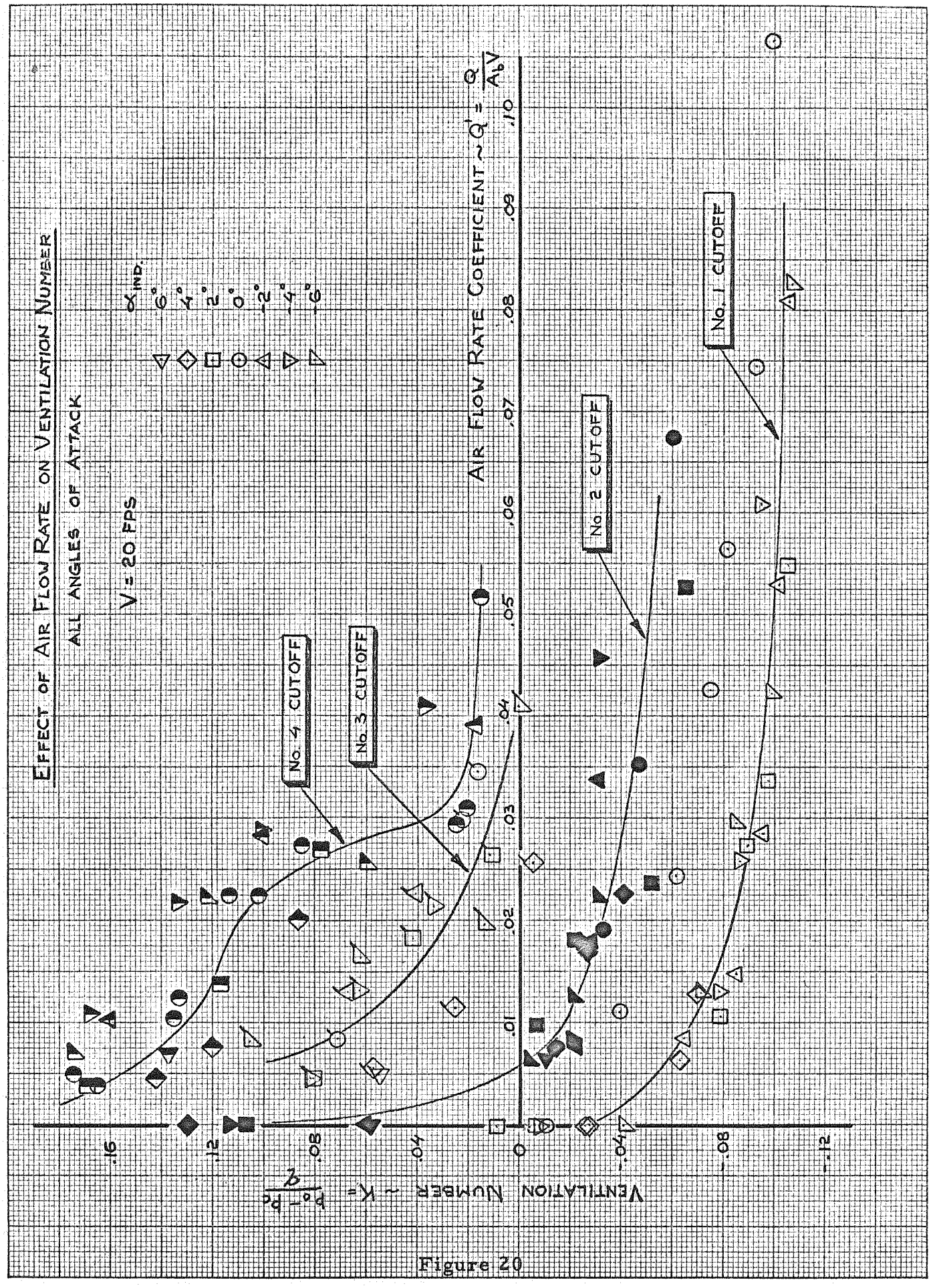
EFFECT OF AIR FLOW RATE ON VENTILATION NUMBER
ALL ANGLES OF ATTACK
V = 20 FPS
α IND.
6°
4°
2°
0°
-2°
-4°
-6°
AIR FLOW RATE COEFFICIENT ~ Q' = Q/AbV
.10
.09
.08
.07
.06
.05
.04
.03
.02
.01
0
-.04
-.08
-.12
.16
.12
.08
.04
VENTILATION NUMBER ~ K = Δp/q
No. 4 CUTOFF
No. 3 CUTOFF
No. 2 CUTOFF
No. 1 CUTOFF

Figure 20

APPENDIX A

Method for Measuring Pressure of a Ventilated Cavity

Measurements of static pressures in water by conventional methods are often difficult when the region of interest is cavitating or ventilating. The water vapor or air will enter and partly fill the tubes leading to the manometer or pressure gage. Such a condition, with both a compressible and incompressible fluid in the pressure lines, will result in erroneous pressure readings. To overcome this difficulty, a scheme was developed at the Laboratory by T. Kiceniuk (as was a similar method by Gadd at NPL, in Reference 10) whereby air at very low pressure constantly filled the pressure lines and slowly bubbled out of the pressure tap. Thus the water is blown out of the line and the manometer indicates the air pressure required to bleed air out of the pressure tap and which is directly related to the static pressure at the tap. Reference 10 gives a very good analysis of this method.

Since the air trickling out of the pressure tap into the cavity should be part of the total air flow, the arrangement indicated in Figure 4 in the main body of this report was used in the present program. With the probe in still air, the pressure regulator B and the throttling valve B were adjusted so that the manometer indicated a pressure of .02 feet of water. Then the tunnel was filled to the reference water level of 1.65 feet, and the static water pressure of the manometer recorded. This static water pressure was used as the reference, P_o. Since this method was erroneously corrected for a non-existant surface tension effect, all cavity pressures reported and plotted are probably about .03 feet high.

During the test it was observed that with sudden changes in the ventilation conditions a small amount of water would still enter the pressure tap. For this reason an additional air line was connected to the pressure lead which would make it possible to purge the system when necessary.

Because the air in the pressure line had to be throttled to a pressure so close to atmospheric, the regulator and valve would be practically closed and difficult to adjust. Small fluctuations in the air pressure were noted as a consequence. For this reason, a method of throttling the air, similar to that described in Reference 10 will be tried in the near future.

APPENDIX B

Reduction of Air Flow Rate Data

The air flow rate into the foil base cavity was measured with the Fisher and Porter Flowrator. This instrument is calibrated to measure the flow rate at standard temperature and pressure. One of two floats can be used in the glass tube of the Flowrator; one is stainless steel, the other is aluminum. The calibration curves, Figures 6 and 7 in the main body of this report show that for the same air flow rate the readings with the aluminum float are larger than those with the stainless steel float. Hence the aluminum float gives higher resolution at small flow rates.

When the air supply line is at a pressure and/or temperature different from standard, a correction has to be made to the meter reading. Consider the following analysis:

Let Q and p, be the air flow rate and pressure in the Flowrator, causing the float to rise to a steady value y. Then:

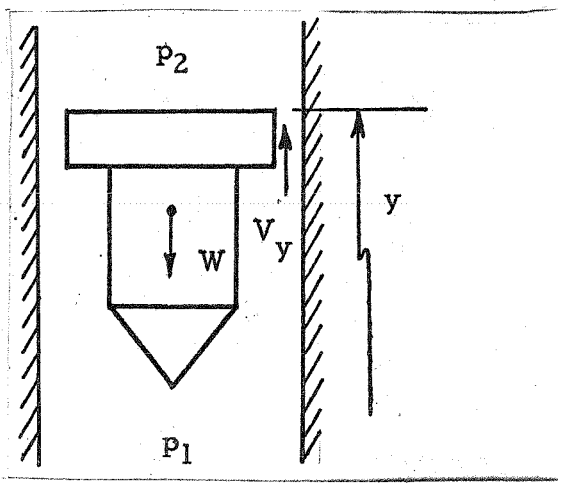

$$W = A_f (p_1 - p_2)$$

$$\text{or} \qquad (p_1 - p_2) = \frac{W}{A_f} = \text{constant}$$

The clearance between the float and wall acts as an orifice, hence:

$$Q = C(A_t - A_f)\sqrt{\frac{1}{\rho}(p_1 - p_2)}$$

$$= (A_t - A_f)\, V_y$$

$$\text{or} \qquad \rho V_y^2 = C^2(p_1 - p_2)$$

where: C = orifice coefficient

A_t = cross sectional area of tube

A_f = cross sectional area of float

ρ = air density at p_1

V_y = air velocity between tube wall and float

When the supply line pressure is other than standard and the flow rate is such that the actual reading y is the same (i.e. the cross sectional area A_t is the same), the weight of the float is still supported by the same pressure difference $(p_1 - p_2)$. Hence:

$$(\rho V_y^2)_{\text{line}} = (\rho V_y^2)_{\text{standard}}$$

and also $$Q_\ell = Q_s \frac{(V_y)_\ell}{(V_y)_s} = Q_s \sqrt{\frac{\rho_s}{\rho_\ell}}$$

$$Q_\ell = Q_s \sqrt{\frac{p_s}{p_\ell}} \qquad (1)$$

The correction for temperature is likewise:

$$Q = Q_s \sqrt{\frac{T_\ell}{T_s}} \quad \text{where T is absolute temperature}$$

The air lines from the Flowrator to the cavity are sufficiently long and the exit at the probe tip large enough that the transition can be assumed to be isothermal. Hence the air flow rate into the cavity (which is at pressure p_c) is:

$$Q = Q_\ell \frac{p_\ell}{p_c} = Q_s \frac{p_\ell}{p_c} \sqrt{\frac{p_s}{p_\ell}} \qquad (2)$$

Since for these tests p_c is almost equal to atmospheric or standard pressure:

$$Q \cong Q_s \sqrt{\frac{p_\ell}{p_s}} \qquad (3)$$

The dimensionless air flow rate coefficient is defined as:

$$Q' = \frac{Q}{VA_b} \qquad (4)$$

where V = free stream velocity
A_b = base area of foil.

APPENDIX C

Preliminary Investigation of Flow Between No. 3 Two-Dimensional End-Plates for Free-Surface Water Tunnel

The two-dimensional working section insert (No. 3) used in this program is shown in Figure 1 of the main body of this report. The detailed drawings and dimensions are presented in N-3296 YY. For a clear, unobstructed view of the flow about models, these end-plates were made of 5/8 inch thick plexiglass attached to stainless steel right angles at the top and bottom and faired stainless steel plates at the leading and trailing edges. By means of threaded rods spanning the two plates at each corner, the distance between the end-plates can be adjusted to suit the model size requirements. This whole structure can be lowered into the test section and bolted down to the bottom of the tunnel.

The preliminary study of the flow characteristics between these end-plates consisted of three parts:

1. Water surface contour
2. Angularity of flow below the water surface
3. Boundary layer growth along the walls

1. Water Surface Contour

With the end-plates set parallel and four inches apart it was observed that at velocities above 10 fps the water surface gradually rose between the end-plates until it was more than two inches higher as it left the trailing edges. In order to measure the contour, a Lory Type A pointer gage was mounted on a piece of channel iron which spanned the top of the working section. The pointer gage was positioned at various distances downstream from the leading edges of the plates and the water surface elevation measured with respect to the bottom of the working section. This was done at velocities of 12 fps and 24 fps. Figure C-1

shows the contours at these two velocities. It should be noted that the abscissa is four times the ordinates, so that the upflow appears exaggerated in this diagram.

The second set of water surface contours was measured with the end-plates separated more at the trailing edges than at the leading edges. Although this made the water surface more nearly level, the non-parallel position of the walls would be quite inconvenient for actual model tests. Since the relative longitudinal position of the model and walls changes with a change in angle of attack, the clearance between the walls and foil tips would vary also if the walls were not parallel. These tip effects could cause a greater source of error than does correction for the direction of flow. For this reason, it was decided to keep the end-plates parallel at all times for this experiment.

2. Angularity of Flow Below the Water Surface

The upflow between the end-plates does not occur near the water surface alone; it extends practically to the bottom of the channel. To measure the angle of upflow at various depths, a thin, black string was suspended from the entrance of the two-dimensional test section. The string was tied to a horizontal nylon string wrapped around both end-plates so that it was transverse to the flow. With the tunnel running at the desired speed, the angle of the trailing, black string was measured by lining up a bar (and its reflected image from the window) with the string and then measuring the angle of the bar. Figure C-2 shows this setup. The bar with its yellow tape on the front edge was set on the swivel head of a tripod. A military surplus protractor, with an adjustable level, calibrated in mills (.001 radians), was put alongside it to measure the angle. Because of fluctuations of the string, the repeatability was about $\pm$ 3 mills or $\pm .17^{o}$. Since the string (like the water surface) was deflected more toward the

downstream end, the angle was measured only at the point of the approximate model location. The depth of the string was measured with a scale at the entrance of the end-plates.

The results of these measurements are shown in Figure C-3. It can be seen that the angle of upflow is quite significant and does not decrease very rapidly with depth. It should be noted also that the upflow is greater for the low velocity (10 fps); this could be caused by angularity in the flow before it enters the two-dimensional working section. For this particular hydrofoil program the foil depth was approximately 8.5 inches and the velocity 20 fps; thus the angle of upflow was very close to 3.0^{o}.

3. Boundary Layer Thickness Along Walls

Because a hydrofoil model mounted between the end-plates would be partly in the wall boundary layer, a preliminary study was made to determine the boundary layer thickness at various positions along the walls and at different tunnel velocities. Since it was undesirable to drill holes in the end-plates, the pitot tube was not brought through the wall but from above through the water surface. At first a 3/16 inch diameter Prandtl pitot tube was used, but because of its thickness and resulting limitations for boundary layer studies, it was later replaced by a 1/16 inch diameter total head tube. The total head tube was mounted on a traversing mechanism which, in turn, was mounted on the elevating mechanism on the top of the tunnel working section. The pressures were recorded on a water manometer.

Three velocities (V = 10, 15 and 20 fps) and four longitudinal locations of the pitot tube (ℓ = 1.0, 9.5, 18.0, 26.0 inches) were used. The distance ℓ is measured from the leading edge of the end-plate and the transverse distance w_o is measured from the inside wall to the centerline of the pitot tube. The tunnel velocity manometer reading was designated p_q on the data sheet; p_t was the reading of the pitot tube manometer and d_s was the depth of

the pitot tube below the water surface.

The velocity profiles thus obtained are shown in Figure C-4. The boundary layer thickness, δ , is also compared with empirical results for turbulent boundary layer along a flat plate presented in Reference 8. Figure C-5 shows the boundary layer growth at the three velocities. The measured δ is greater than was expected, particularly near the leading edge. The distance from the wall could not be measured very accurately because the probe was mounted from above and would vibrate somewhat. It is intended to make a more precise survey in the near future by bringing a pitot tube through the end-plates. Thus vibration of the probe would be reduced considerably and the boundary layer could be measured more accurately.

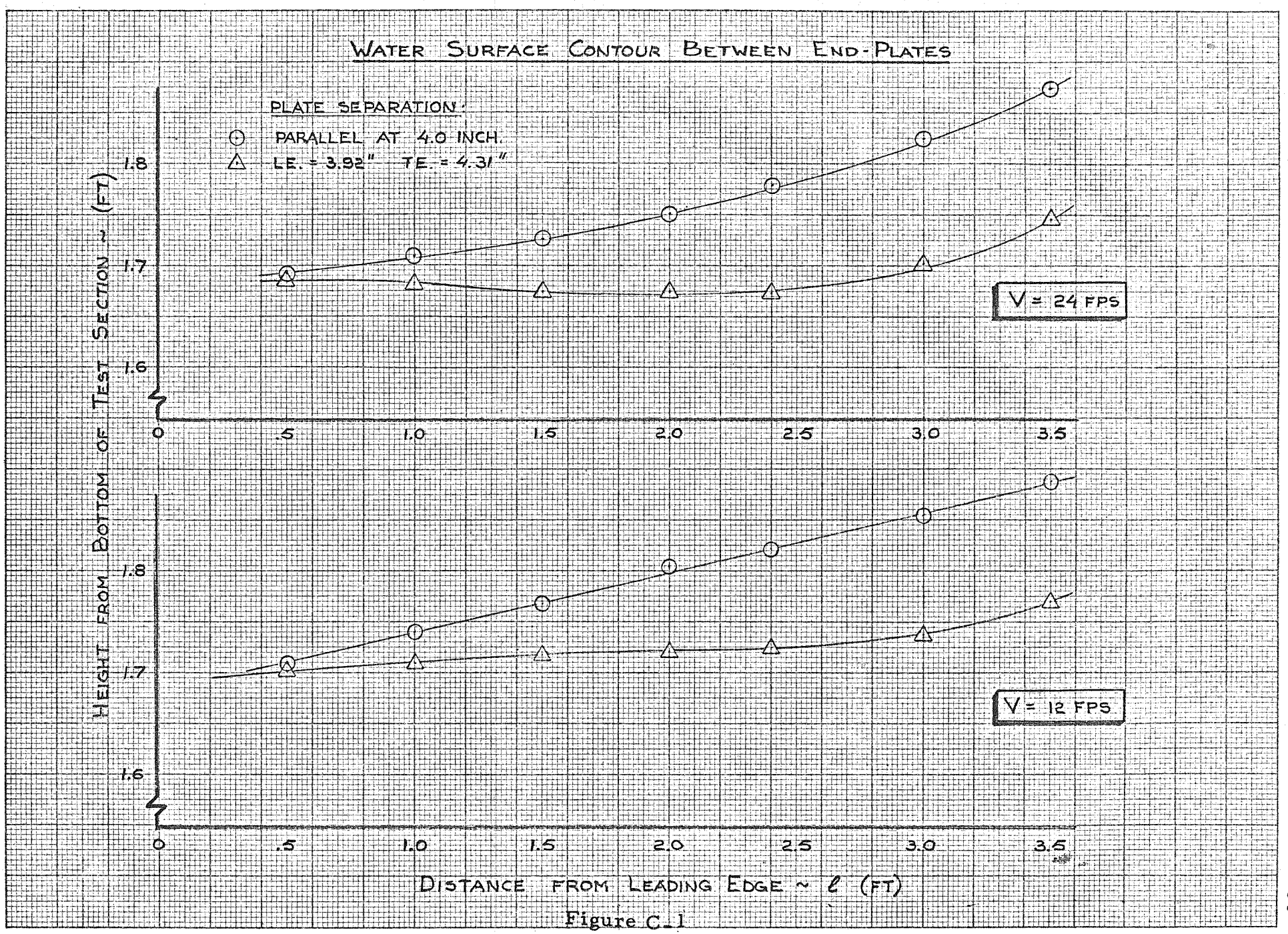
WATER SURFACE CONTOUR BETWEEN END-PLATES
PLATE SEPARATION:
PARALLEL AT 4.0 INCH.
L.E. = 3.92" T.E. = 4.31"
V = 24 FPS
V = 12 FPS
HEIGHT FROM BOTTOM OF TEST SECTION ~ (FT)
1.8
1.7
1.6
0
.5
1.0
1.5
2.0
2.5
3.0
3.5
DISTANCE FROM LEADING EDGE ~ ℓ (FT)

Figure C_1

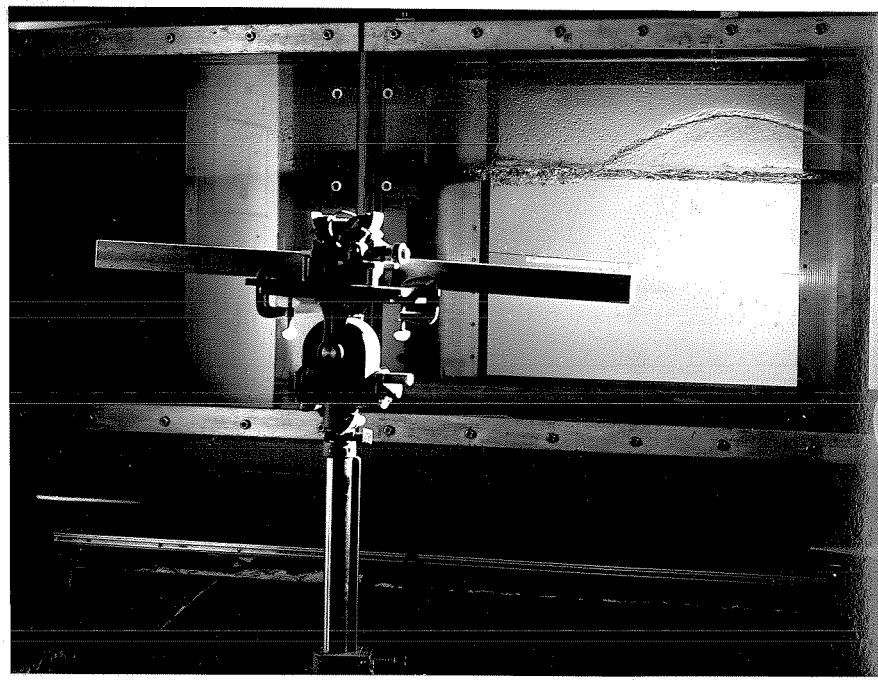

Figure C-2 - Method Used to Measure Angle of Upflow in Two-Dimensional Working Section. Shown Are the Black String, the Steel Bar with Its Image and Protractor Mounted on the Tripod

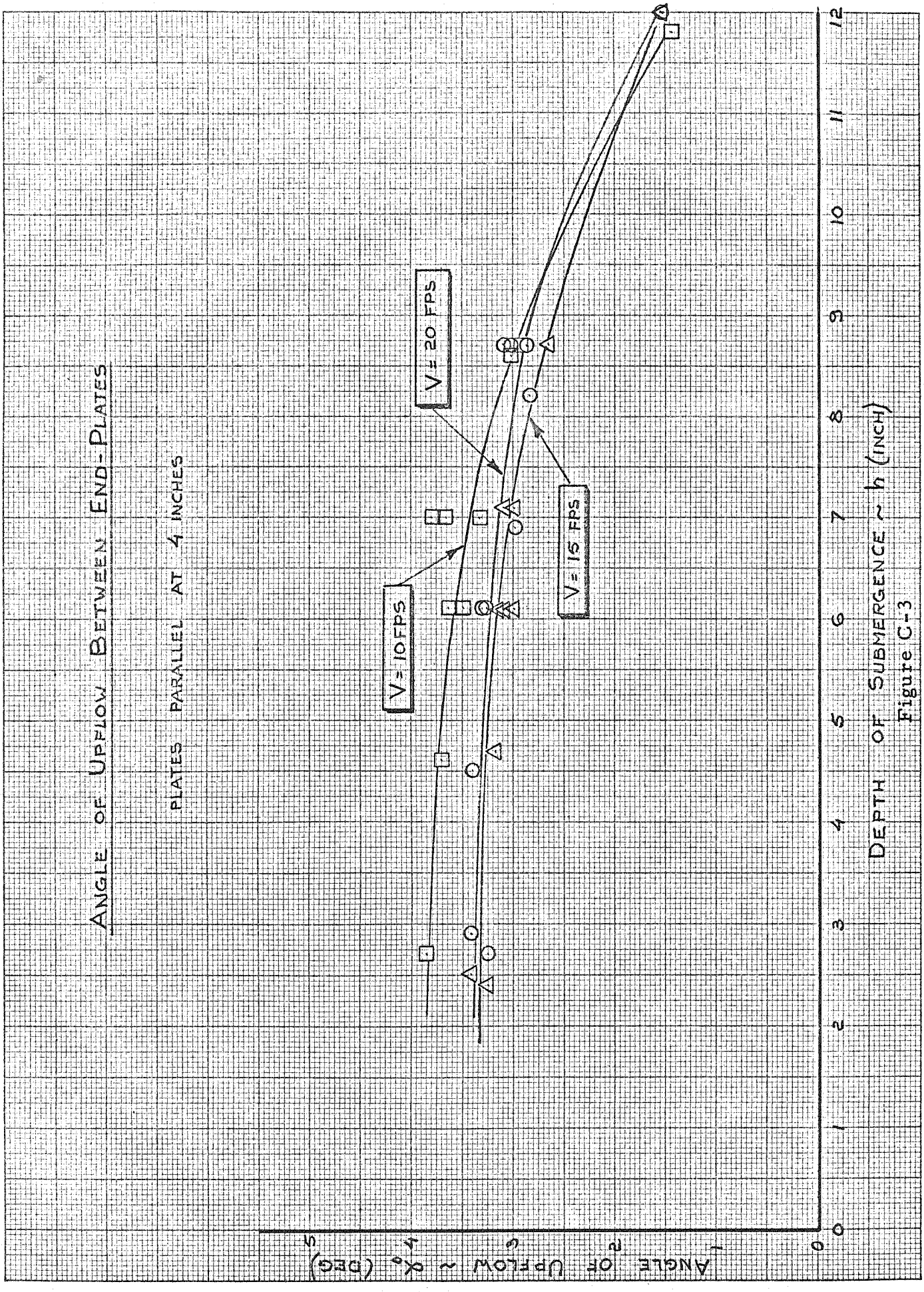
ANGLE OF UPFLOW BETWEEN END-PLATES
PLATES PARALLEL AT 4 INCHES
V = 10 FPS
V = 20 FPS
V = 15 FPS
ANGLE OF UPFLOW ~ γ_s (DEG)
DEPTH OF SUBMERGENCE ~ h (INCH)
0
1
2
3
4
5
6
7
8
9
10
11
12

Figure C-3

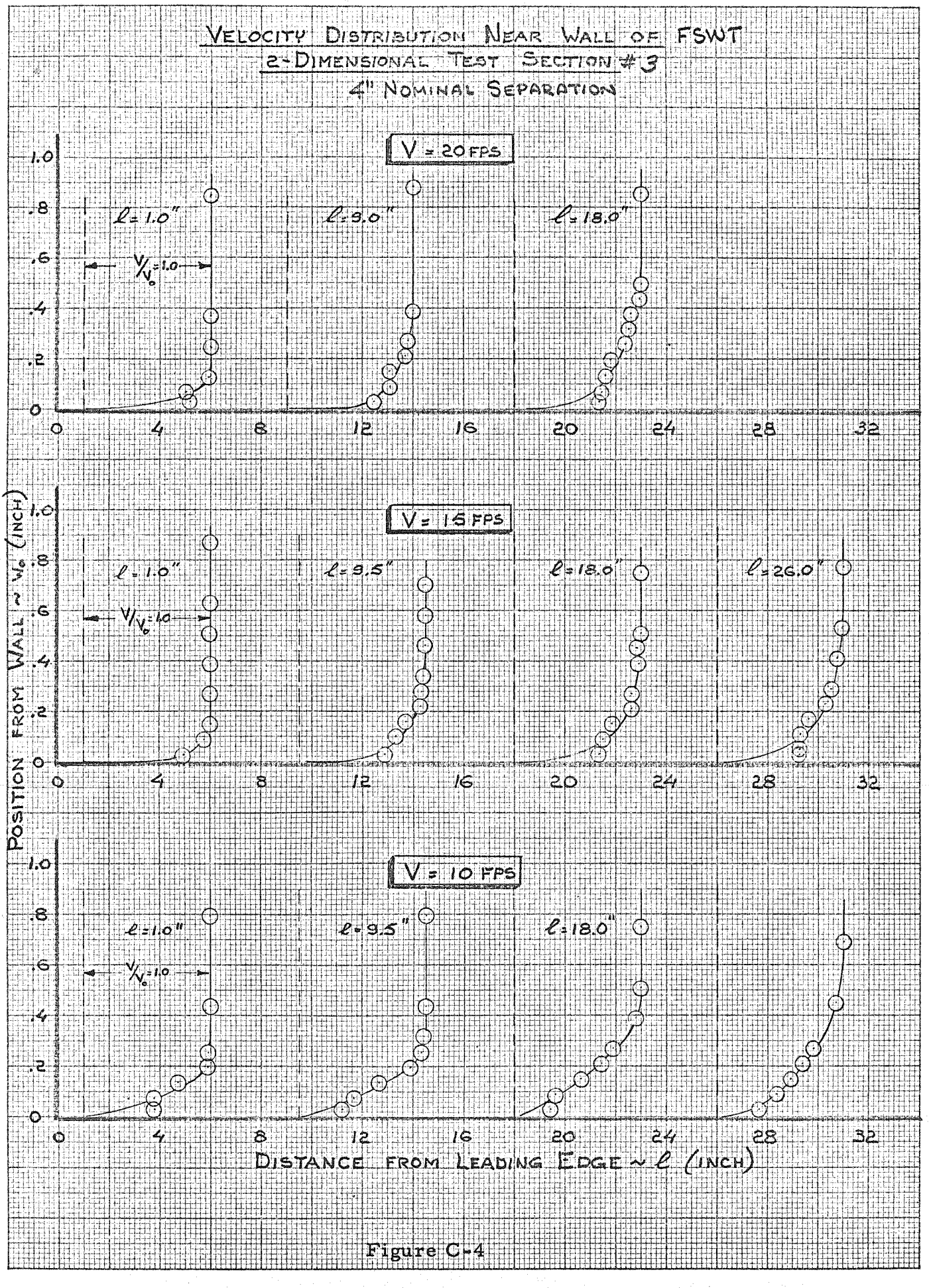
VELOCITY DISTRIBUTION NEAR WALL OF FSWT
2-DIMENSIONAL TEST SECTION #3
4" NOMINAL SEPARATION
V = 20 FPS
ℓ = 1.0"
ℓ = 9.0"
ℓ = 18.0"
V/V∞ = 1.0
V = 15 FPS
ℓ = 1.0"
ℓ = 9.5"
ℓ = 18.0"
ℓ = 26.0"
V/V∞ = 1.0
V = 10 FPS
ℓ = 1.0"
ℓ = 9.5"
ℓ = 18.0"
V/V∞ = 1.0
POSITION FROM WALL ~ y/y∞ (INCH)
DISTANCE FROM LEADING EDGE ~ ℓ (INCH)
0
.2
.4
.6
.8
1.0
4
8
12
16
20
24
28
32

Figure C-4

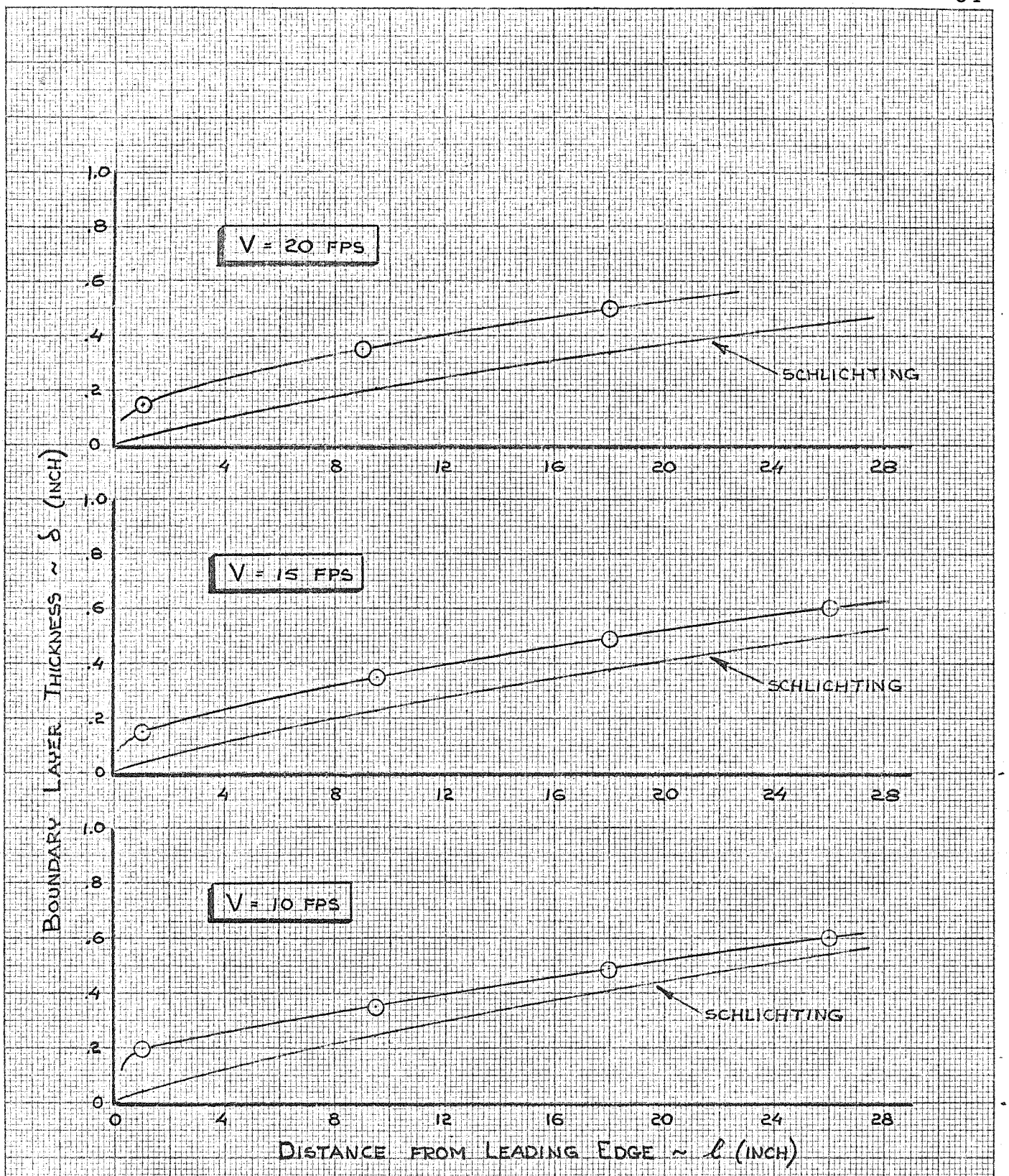

BOUNDARY LAYER GROWTH ALONG
END-PLATES (2-D INSERT #3)
4" NOM. SEPARATION

APRIL 1962

RB.

Figure C-5

plates distance
LE = 3 59/64"
TE = 4 5/16"

HYDRODYNAMICS LABORATORY
TEST DATA SHEET

EXP. ____ RUN ____ PAGE 65

DATE 10 - 31 - 61

TEST ____

VELOCITY 12 fps GEAR BOX ____

OBSERVERS ____

MODEL INSTALLATION NO. ____

NOSE NO. ____ AFTERBODY NO. ____ MODEL NAME ____

Po ____

INDEXES ____

$h_{ref} = 1.565 - .349 = 1.216$

Bo ____ TW ____ Pv ____

VERT. RUDDERS ____

WORKING SECTION ____

HORIZ. RUDDERS ____

SHIELD NO. ____ DATA FILM ____

ADAPTER NO. ____ PHOTOGRAPHS ____

JOB NO. ____

	l inch	d, ft 12 fps			d, 24 fps				
.5	6.0	.485	1.701		.468	1.684			
1.0	12.0	.494	1.710		.467	1.683			
1.5	18.0	.501	1.717		.458	1.674			
2.0	29.0	.504 (av.)	1.720		.458	1.674			
2.4	29.0	.509	1.725		.468	1.684			
3.0	35.0	.522	1.738		.487	1.703			
3.4	40.5	.555	1.771		.530	1.746			
plates // at 4"									
	l	12 fps. d1							
	6.0	.493	1.709		476	1.692			
	12.0	.525	1.741		.491	1.707			
	18.0	.551	1.767		.511	1.727			
	24.0	.589	1.805		.535	1.751			
	29.0	.606	1.822		562	1.778			
	35.0	.640	1.856		608	1.824			
	40.5	.671	1.887		658	1.874			

HYDRODYNAMICS LABORATORY
TEST DATA SHEET

EXP. ____ RUN ____ PAGE ____

DATE Oct 28, '61

TEST 2-Dim, Surface deflection

OBSERVERS ____

VELOCITY ____ GEAR BOX ____

MODEL INSTALLATION NO. Spacing 4.00 inches, both ends

d_1 center (between plates)

NOSE NO. ____ AFTERBODY NO. ____ MODEL NAME ____

d_2 port side

P_o ____

INDEXES ____

d_3 stard. side

B_o ____ TW ____ Pv ____

VERT. RUDDERS ____

ℓ dist from L.E. plates

WORKING SECTION ____

HORIZ. RUDDERS ____

SHIELD NO. ____ DATA FILM ____

ADAPTER NO. ____ PHOTOGRAPHS ____

JOB NO. ____

V	Vel. fps	ℓ inch	d_1 ft	d_2	d_3				
	~~9.0~~	6.0	~~.350~~						
		12.0	.353						
		~~18.0~~	~~.370~~						
				.452					
	12.0	6.0	.490	.481	489				
		12.0	.519	.505	509				
		18.0	.550	.521	525				
		24.0	.582	.536	532				
		29.0	.601	.535	547				
		35.0	.635	.529	.536				
		40.5	.667	.509	493				.177
		48.0	.667	.419	.448				
		54.0	.625	.397	.408				

Upflow in Two-Dimensional Test Section F.S.W.T. Jan. 9+10, 62 67

SB.

Remarks		V fps	h_{LE} inch	h model pos inch	α_o mills	α_o deg	h_{TE} inch			
		10	4.6		64.5	3.70	4.9			
		15	4.7		55.5	3.18	4.6			
		20	4.5		59.5	3.41	4.3			
		10	8.6		52	3.03	9.6			
		15	8.1		40	2.29	9.1			
		20	8.2		49.5	2.84	8.9			
	(	10	11.8		25	1.43				
		15	12		26.5	1.52				
		20	12		27	1.55				
		10	1.5		37	2.12 (?)	x1.0			
		15	2.4		57	3.26	2.6			
		20	2.7		57	3.26	2.5			
Jan 10.		10	2.7	3.0	67	3.87		1 stairm pump		
Tunnel filled to 1.64 ft		"	2.7		67	3.87		2 stairm pump		
		15	2.5	2.9	60	3.44				
		20	2.9	3.0	60	3.44				
		"	2.9		60	3.44				
		15	6.1	6.1	53.5	3.07				
		"	"		52	2.98				
		"	"		58	3.32				
		"	"		55	3.15				
		10	6.1		61	3.5				
		"	"		63.5	3.64				
		"	"		61	3.5				
		"	"		63.5	3.64				
		20	6.1	6.2	55	3.15				
		"	"	"	58	3.32				
		"	"	"	57	3.27				
		20	6.9	7.1	52	2.98				
		15	7.1	7.0	54	3.09				
		"	"	"	52	2.98				
		10	7.0		66	3.78				
		"	"		58	3.32				
		"	"		64	3.67				

Upflow in Two-Dimensional Test Section FSWT.

Jan 10, 68

BB.

V fps	h_{LE} inch	h inch model/prototype	α_0 millirad	α_0 degrees	h_{TE} inch
10	8.7	8.9	52	2.9 (av)	
"	"	"	48.5		
"	"	"	51		
15	8.7	9.0	46 (3x)	2.64	
20	8.7	9.0	50	2.87	
"	"	"	54	3.10	
"	"	"	53	3.06	

Total Head Survey Near Wall

FSWT
11-10-61

	ℓ in	w ft	p_g ft	P_t ft		H_o	V (fps)	w_o in.	V/V_o				
static	9.5	.164 ± .5	1.548	.150	=								
$V_o \approx 10$ fps	9.5	.164	3.22	1.02	5.4 in	.170	3.37	.030	.341				
		.160	3.22	1.14		.990	4.34	.078	.439				
		.155	3.21	1.38		1.230	6.26	.138	.634				
		.150	3.20	1.56		1.410	7.71	.198	.78				
		.145	3.21	1.77		1.620	9.40	.258	.951				
		.140	3.21	1.80		1.650	9.64	.318	.975				
		.130	3.20	1.83		1.680	9.88	.438	1.00				
		.100	3.21	1.83		1.680	9.88	.798	1.00				
	1.0	.164	3.22	1.26	≈ 5	1.110	5.56	.030	.553				
		.160	3.19	1.245		1.095	5.44	.078	.540				
		.155	3.20	1.51		1.360	7.57	.138	.752				
		.150	3.20	1.80		1.650	9.90	.198	.984				
		.145	3.20	1.80		1.650	9.90	.258	.984				
		.130	3.20	1.815		1.665	10.02	.438	1.00				
		.100	3.20	1.82		1.670	10.06	.798	1.00				
	18.0	.160	3.19	.98	≈ 6.0	1.130	2.65	.030	.384				
		.155	3.20	1.61		1.760	2.09	.090	.304				
		.150	3.19	1.26		1.410	4.90	.150	.524				
		.145	3.19	1.45		1.602	6.42	.210	.686				
		.140	3.19	1.56		1.710	7.31	.270	.782				
		.130	"	1.77		1.900	8.77	.390	.960				
		.120	3.20	1.81		1.942	9.31	.510	.996				
		.100	3.20	1.82		1.955	9.35	.750	1.00				
	26.0	.155	3.20	.96	≈ 7	.810	3.36	.030	.330				
		.150	3.19	1.14		.990	4.80	.090	.472				
		.145	3.19	1.28		1.130	5.93	.150	.583				
		.140	3.20	1.39		1.240	6.81	.210	.670				
		.135	3.19	1.51		1.360	7.77	.270	.764				
		.120	3.19	1.735		1.585	9.58	.450	.941				
		.100	3.19	1.81		1.660	10.18	.690	1.00				
		.050	3.18	1.81		1.660	10.18	1.290	1.00				

69

Total Head

18 Nov. 15, '6
FSWT

	ℓ in	w ft	p_q ft	p_t ft	p_{st}	d_s in	p_{to}	Δh_{H_2O} (ft)	V fps	W_o (in)	Y/N_o
V ≈ 15 fps	9.5	.176	5.15	~~1.94~~		4.8	1.880	1.647	10.29	.030	.679
		.170		~~3~~ 2.35			2.290	2.057	11.52	.102	.761
		0.165	5.16	2.84			2.780	2.547	12.82	.162	.847
		0.160	5.17	3.455			3.395	3.162	14.45	.292	.954
		0.155	5.17	3.60			3.540	3.307	14.62	.282	.965
		.150	5.18	3.73			3.670	3.437	14.88	.342	.982
		.140	5.18	3.82			3.760	3.527	15.08	.462	.995
		.130	5.22	3.835			3.775	3.542	15.11	.582	1.00
		.120	5.23	3.85			3.790	3.557	15.13	.702	1.00
		.100	5.20	3.83			3.770	3.537	15.10	.942	1.00
		.060	5.21	3.84			3.780	3.547	15.11	1.422	1.00
	1.0	.060	5.16	3.78		4.0	3.720	3.553	15.12	1.350	.994
		.100	5.16	3.785			3.725	3.558	15.13	.870	.994
		.120	5.16	3.80			3.740	3.573	15.18	.630	.995
		.130	5.17	3.795			3.735	3.568	15.17	.510	.995
		.140	5.20	3.81			3.750	3.583	15.20	.390	1.00
		.150	5.20	3.82			3.760	3.593	15.22	.270	1.00
		.160	5.20	3.82			3.760	3.593	15.22	.150	1.00
		.170	5.19	2.48			2.420	2.253	12.04	.030	.790
		.165	5.20	3.52			3.460	3.293	14.56	.090	.955
	18.0	0.160	5.22	1.86		5.0	1.800	1.550	10.00	.030	.661
		0.155	5.20	2.00			1.950	1.700	10.48	090	.692
		.150	5.22	2.42			2.360	2.110	11.68	.150	.772
		.145	5.22	3.27			3.210	2.960	13.82	.210	.915
		.140	5.22	3.26			3.220	2.970	13.84	.270	.915
		.130	5.22	3.75			3.690	3.440	14.90	.390	.985
		.135	5.22	3.65			3.590	3.340	14.67	.450	.970
		.120	"	3.84			3.780	3.530	15.10	.510	1.00
		.100	"	"			3.780	3.530	15.10	.750	1.00

170

Total Head

JB. Nov. 16, '61
ESWT

	ℓ (in)	w ft	p_g ft	p_t ft	d_s in	P_{t_0}	Δh (ft H_2O)	V fps	w_o (in)	V/V_o
$V \approx 15$ fps	26.0	.162	.527	1.78	4.5	1.720	1.512	9.88	.030	.645
		.160	"	1.78		1.720	1.512	9.88	.054	.645
		~~.155~~	~~.524~~	~~2.49~~						
		.150	.524	2.14		2.080	1.872	10.98	.174	.715
		~~.150~~	~~.524~~	~~2.49~~						
		.155	"	1.86		1.740	1.532	9.94	.114	.649
		.145	.526	2.92		2.860	2.652	13.08	.234	.854
		.140	"	3.20		3.140	2.932	13.76	.294	.898
		.130	.530	3.61		3.550	3.342	14.66	.414	.956
		.120	.530	3.81		3.750	3.542	15.11	.534	.987
		.100	"	3.89		3.830	3.622	15.29	.774	1.00
		.060	"	3.96		3.840	3.632	15.30	1.254	1.00
static				.060	2.0					

Boundary Layer Pitot Tube (Total Head) Survey — JB. — Nov 25, '64 — 36

Remarks	ℓ (in)	W ft.	p_g ft	p_t ft H_2O	d_{pt} (in)	p_g ft Check	$p_{t_o} - p_{st}$ ft H_2O	V fps	w_o (in)	V/V_o
V∞ 20 fps.	Static		~~1.60~~	~~1.598~~	~~3.0~~					
Mercury Compensated Manometer used for total head readings	static		1.630	1.620	3.2					
~~intermediate~~	9.0	.171	8.16	4.84	4.0	8.23	3.145	14.20	.031	.691
		.166	8.13	6.10	4.1	8.21	4.405	16.83	.091	.820
		.161	8.20	6.12	4.1	8.23	4.425	16.88	.151	.821
		.156	8.22	7.45	4.1	8.22	5.755	19.22	.211	.935
		.151	8.25	7.75	"	8.24	6.055	19.72	.271	.960
		.141	8.24	8.23	"	8.20	6.535	20.53	.391	1.00
		.100	8.20	8.23	"	8.25	6.535	20.53	.883	1.00
	1.0	.100	8.26	8.28	4.0	8.25	6.593	20.60	.847	1.00
		.140	8.30	8.28	"	8.26	6.593	20.60	.367	1.00
		.150	8.28	8.30	"	8.28	6.613	20.63	.247	1.00
		.160	8.35	8.15	"	8.35	6.463	20.39	.127	.989
		.165	8.40	5.96	"	8.32	4.273	16.59	.067	.805
		.168	8.34	6.28	"	8.37	4.593	17.19	.031	.833
	18.0	.169	8.30	4.70	4.4	8.35	2.98	13.85	.031	.668
		.166	8.17	4.82	"	8.30	3.10	14.12	.067	.681
		.160	8.35	5.08	"	8.34	3.36	14.71	.139	.710
		.155	8.40	5.55	"	8.40	3.83	15.70	.199	.758
		.150	8.40	6.55	"	8.40	4.83	17.61	.259	.850
		.145	8.40	7.05	"	8.40	5.33	18.53	.319	.895
		.140	8.42	7.30	"	8.42	5.58	18.91	.379	.913
		.130	8.40	8.42	"	8.42	6.70	20.77	.499	1.00
		.135	8.40	8.24	"	8.42	6.52	20.48	.439	.989
		.100	8.40	8.42	"	8.40	6.70	20.77	.859	1.00
	static		1.60	1.605	3.0					

72

DISTRIBUTION LIST

Copy No. 1 - Original Copy - Tunnel Operations Office

2 - File Copy - Hydrodynamics Laboratory Office

3 - Library Copy

4 - Working Copy - Tunnel Operations Office

5 - Mr. A. J. Tickner, Head,
Guidance and Control Division,
U. S. Naval Ordnance Test Station,
Pasadena, California

6 - Thomas G. Lang (P5006), Head,
Hydrodynamics Group, U. S. Naval Ordnance
Test Station, Pasadena, California

7 - Supernumerary Copy